Multi-Color and Multi-Material 3D Printing of Knee Joint Models

Oliver Grimaldo Ruiz (oliver.ruiz0809@gmail.com)
Politecnico di Torino https://orcid.org/0000-0001-5901-0092
Yasin Dhaher
UT Southwestern: The University of Texas Southwestern Medical Center

Research

Keywords: Three-dimensional printing, Knee Joint, Patient-specific anatomical models, Anterior cruciate ligament reconstruction, Total knee arthroplasty

Posted Date: September 23rd, 2020

DOI: https://doi.org/10.21203/rs.3.rs-78803/v1

Version of Record: A version of this preprint was published at 3D Printing in Medicine on April 29th, 2021.
See the published version at https://doi.org/10.1186/s41205-021-00100-0.

Multi-color and Multi-Material 3D Printing of Knee Joint models

Oliver Grimaldo Ruiz [1], Yasin Dhaher [2]

1. Department of Structural, Geotechnical and Building Engineering (DISEG), Politecnico di Torino, 10129 Turin, Italy.

Contact: +39 3337933976.

E-mail: oliver.grimaldo@polito.it

URL: http://www.diseg.polito.it/en/personale/scheda/(nominativo)/oliver.grimaldo

2. Physical Medicine and Rehabilitation, Orthopaedic Surgery, UT Southwestern Medical Center, 5323 Harry Hines Blvd, Dallas, TX 75390, USA.

Contact +1 214-648-0007.

E-mail: yasin.dhaher@utsouthwestern.edu

URL: https://profiles.utsouthwestern.edu/profile/175158/yasin-dhaher.html

Abstract

Background Every year, 3DP provides more alternatives and solutions in the medical field. Applications such as custom-made prosthetics and implants, platforms for pharmaceutical research, and PSAMs are the immediate emerging trends. Certainly, 3DP advancement is the convergence of multiple factors including improvements in medical software, 3D printer evolution, availability of new printing materials, improved industry support, and increasing commitment from medical societies and regulators. The overarching theme of this study is centered on exploring possible PSAMs and 3DP applications for improving surgical outcomes in orthopedics, particularly in ACL-R as well as providing functional models for TKA.

Methods 3-Matic, Rhinoceros, and SolidWorks were used to create three 3D computer-generated PSAMs: (1) Knee Joint model, wherein collagen fibers matrix structure is mimicked, (2) ACL-R model using a BPTB graft, incorporating key surgical outcomes such as orientations-architecture and positions-dimensions of the tunnels, as well as a custom-made SG based on patella anatomy (3) TKA model considering custom-made CS implants with symmetric tibial bearing design. Before printing, mechanical uni-axial tensile tests of materials were conducted using an Instron S3300, following the ASTM designation D412-C. The printing materials selection process and matching with anatomical structures were based on

the analysis of the mechanical pattern of the strain-stress curves from different combinations of Agilus30™. The Stratasys J750™ printer was used to manufacture the ACL-R model (previous study), the ACL-R model with SG, and the TKA model.

Results The combinations No. 1-4 were chosen for 3DP with elastic modules of 1.8-0.7 MPa and Pearson coefficients of 0.980-0.991 respectively. The PSAMs were tested manually simulating 50 flexo-extension cycles without presenting ruptures, custom-made SG matches perfectly with PT anatomy.

Conclusion Functional PSAMs were printed with high fidelity, considerable cost, and short duration from planning to manufacturing. These coincided completely with 3D computer-generated PSAMs replicating fibers and features of the Knee Joint anatomy. The proposed PSAMs can be considered as an alternative to replacing cadaver specimens for medical training, pre-operative planning, education purposes, and validation of predictive models. We highlight the potential of PolyJet manufacturing combined with specialized medical software as a path to change the way specialists and researchers plan, execute, and validate complex procedures.

Keywords Three-dimensional printing, Knee Joint, Patient-specific anatomical models, Anterior cruciate ligament reconstruction, Total knee arthroplasty.

Background

Additive manufacturing (AM) also widely known as three-dimensional printing (3DP) is an emerging and revolutionary technology that is getting substantial interest in several key areas such as the automotive, aerospace, military, and medical fields. The 3DP process is based on the principle of layered manufacturing, in which materials are overlapped layer-by-layer enabling the build of 3D objects (1). Nowadays, the impact of 3DP in the medical field has acquired considerable relevance in the scientific and academic communities owing to its potential and wide range of applications. However, the 3DP role in medicine is not recent, this has been reported since the early 1990s and in recent years, there has been a considerable rise in the number of emerging trends in the field, demonstrated by the growing body of literature featuring clinical work and medical research (2). The 3DP advancement is the result of the convergence of multiple factors, including improvements in medical software, 3D printer evolution, the availability of new

printing materials and improved industry support, and increasing commitment from medical societies and regulators (3). Current research applications are classified into the following five main areas of focus: (1) Patient-specific anatomical models (PSAMs), (2) Custom-made prosthetics and implants, (3) Local bioactive and biodegradable scaffolds, (4) Pharmaceutical research, and (5) Research on directly printing tissues and organs with complete life functions. Although, such applications remain far from widespread in clinical use due to several technical and scientific issues that are currently under study (4).

In particular, PSAMs manufacturing is becoming increasingly popular and accessible due to its application in pre-operative planning, surgical treatment analysis, medical training, and education and research purposes (5). The 3D computer-generated PSAMs are based on digital imaging and communications in medicine (DICOM) file formats, data derived from several acquisition modalities such as computed tomography (CT), magnetic resonance imaging (MRI), and ultrasound (US) (6). The DICOM file formats must be converted into a format, which can be recognized by the 3D printer. Therefore, first, it is uploaded into a program (e.g. Mimics, 3D Slicer, OsiriX) which enables segmentation and 3D reconstruction of the images. It is then exported in a standard triangle language (STL) file format making it readable by computer-aided design (CAD) and computer-aided engineering (CAE) software, which are used for design and simulation. Finally, 3D objects are created by repetitively moving the print head in the Z-direction and depositing the desired material into layers sequentially (7). The PSAMs have been utilized extensively in the area of orthopedics, providing essential information such as sizes, directions, positions, angulations, and conditions of the bones and surrounding tissues. Researchers and surgeons use this preliminary knowledge for studying complex cases, teaching students and patients, rehearsing the procedures in risk-free settings, pre-procedure designing of grafts and implants, performing finite element analyses, development of simulators, and examination platforms (8,9).

Multiple authors describe the significant role of the PSAMs in three main domains of orthopedics: trauma, degenerative disorders, and oncology (10–12). In the Knee Joint, the most investigations conducted are focused predominantly on total knee arthroplasty (TKA) and their importance in the development of patient-specific prostheses (PSP), instrumentation (PSI) and custom-made implants (13–15).

Nevertheless, anterior cruciate ligament (ACL) tear remains the most frequently intra-articular performed surgery in orthopedic trauma (16,17). Despite its prevalence and impact, the number of publications about the PSAMs and 3DP applications in ACL reconstruction (ACL-R) has been relatively unexplored. The design of patient-specific ACL femoral tunnel guide (18) and a method of accurate bone tunnel placement for ACL-R (19) are the publications highest highlighted. This statement does not consider other important studies and contributions about surgical and computational simulations based on 3D computer-generated PSAMs.

The ACL-R aims to restore physiological joint biomechanics in symptomatic knee instability as well as prevent secondary damage to other structures, such as the cartilage and menisci (20–22). Critical factors such as post-operative traumatic injuries, lack of graft incorporation, loss of motion, and surgical technical errors (surgical technique and surgeon skills) are some of the problems associated with unsatisfactory medium-long-term clinical outcomes (23,24). Moreover, several studies have reported the rise of re-rupture cases due to graft failure and the development of premature degenerative diseases such as osteoarthritis (OA) (25–30). The ACL-R has undergone major advances in the last years. Nowadays, different tendon autogenous options exist for the ACL-R. However, the bone-patellar tendon-bone (BPTB) and the semitendinosus-gracilis (STG) are the most commonly used and are most successful as alternatives. Each type of graft is associated with inherent risks and benefits. Therefore, there is no "ideal" graft to use for ACL-R (31–33). The success or failure of the graft depends on several surgical parameters including graft stiffness, dimensions and pre-tensioning, tunnel placement and orientation, and donor-site morbidity (non-modifiable) (34). Currently, surgical simulations incorporate detailed biomechanical parameters associated with realistic predictions with the potential to improve clinical outcomes of the surgery. However, surgical expertise and pre-operative planning are crucial factors in the ACL-R outcome.

Despite all the recent advances in the technical aspects, traditional ACL-R methods have proven to be the better option to restore pre-injury activity levels. Additionally, there is mixed evidence about the effect of ACL-R on the development of premature OA (35). Structural changes combined with medium and long-term changes in the dynamic load of patients who have undergone a deficient ACL-R contribute significantly (36). Thus far, there are no available interventions-

treatments to restore degraded structures or decelerate disease development. During OA progression, the entire joint organ is affected, including cartilage, bone, synovial tissues, ligaments, and meniscus (37). In an advanced stage, TKA is considered as the most suggested surgical procedure to restore mechanical axes, correct alignment, and soft-tissue balance. Although in several cases, TKA has satisfactory functional and cost-effective outcomes there is significant variability and globally higher revision rates. Most failures can be attributed to the choice of replacement components, fixation of the cement-implant interface, incorrect ligament balance or incorrect alignment, surgical technique and experience, and post-operative care (38). Due to their potential, the PSAMs and 3DP applications may improve intra-operative outcomes, problems associated with graft-failure, recognition of nonanatomic tunnels, surgical technical errors, and reduce the risk of developing OA of the reconstructed knee.

The overarching theme of this study is centered on exploring possible PSAMs and 3DP applications for improving surgical outcomes in orthopedics, particularly in ACL-R as well as providing functional models for TKA.

We manufactured and evaluated three multi-color and multi-material Knee Joint functional models, specifically focusing on the design of a collagen fibers matrix that mimics the hierarchical structure of specialized connective soft tissues. We aimed to take advantage of the capability of the Stratasys J750™ printer combined with medical software Materialise 3-Matic. Our models integrated key surgical outcomes of the ACL-R computational framework using a BPTB auto-graft and a custom-made surgical guide for avoiding graft tunnel length mismatch. Furthermore, we created a model affected by the advanced stage of OA with soft tissues involvement. In our design, we considered a custom-made cruciate sacrificing (CS) implants with symmetric tibial bearing design, we adapted and assembled the PSP components simulating a TKA procedure.

The methodology reported for the production of the multi-material PSAMs might be considered as a new avenue to develop models for replacing cadaver specimens for medical training, research and education purposes, pre-operative planning, and validation of computational predictive models.

Materials and Methods

Multi-color and multi-material three-dimensional printing.

The present study was developed in the Shirley Ryan Abilitylab research hospital which has a Stratasys J750™ (Stratasys, Eden Prairie, MN) multi-color and multi-material 3D printer. The system is by far one of the most advanced technologies of 3D multi-material printing. This uses PolyJet AM technology to manufacture highly realistic and functional prototypes with sharp precision, smooth surfaces, and fine details in a wide range of materials with variable durometers and the possibility of choosing between 360,000 color combinations.

There are many types of 3D printers available, which use a variety of media, substrates, and printing technologies. In particular, the Stratasys J750™ uses ultraviolet (UV) radiation for curing layers of jetted photopolymer. The jetting head is formed by a matrix of jetting orifices disposed along the Y-axis and is mounted on a carriage that allows for X forth-and-back displacements and alternate transverse Y relocations. Subsequently, the manufacturing tray moves in the vertical Z direction, after each layer has been successfully manufactured (39).

The Stratasys J750™ has a large manufacturing tray; the maximum build size of a prototype is 490 x 390 x 200 mm (19.3 x 15.35 x 7.9 in.) The system enables simultaneously mixing up six different materials. In addition to the potential of adjusting material hardness according to shore A scale, other capabilities including accuracy of up to 0.2 mm and smaller layer thickness (LT) of 0.014 mm. The system has three print modes in line with the desired surface finish, production time, and the number of materials incorporated. (1) High Quality six different materials (0.014mm LT), (2) High Mix six different materials (0.027mm LT) and (3) High Speed three different materials (0.027mm LT).

The print materials available have special features such as translucency, flexibility, resistance to UV rays, high temperature, and deflection. Resins are capable of simulating properties ranging from rubber-like to transparent, even high toughness. The system has two main families: Digital model and Model materials, the first one including engineering plastic acrylonitrile butadiene styrene (ABS) in their versions Digital ABS Plus - Digital ABS2 Plus™ (main material used in Fused Deposition Modeling (FDM) technology). The second one includes primary materials options: Vero™ family (rigid opaque materials), RGD525™ (high-temperature resistant materials), DurusWhite™ (simulated polypropylene materials), Tango™-Agilus30™ (rubber-like materials) and VeroClear™ - RGD720 (transparent materials).

The Stratasys J750™ provides many AM advantages, such as the incorporation of multiple colors and materials in a single project, optimization of printing time, easy support material removal (waterjet removal), and easy operation.

Image data management.

Three 3D computer-generated PSAMs were created: (1) Knee Joint model (with a collagen fibers matrix structure), (2) ACL-R model, and (3) TKA model. They were based on standard triangle language (STL) files corresponding to a PSAM of the right male Knee Joint (34). The PSAM incorporates patello-femoral (PF) and tibio-femoral (TF) joints. The following anatomical structures are included: femur, tibia, patella, fibula, major ligaments, articular cartilage, menisci, retinacula, and patella and quadriceps tendons (PT-QT). The 3D computer-generated PSAMs were developed in Materialise 3-Matic (Materialise NV, BE), a design and meshing software for anatomical data. They were exported in STL format to the CAD software SolidWorks, (Dassault Systèmes, France) where they were converted to SolidWorks part file (SLDPRT) format, before being assembled through the same application. The SolidWorks final assembly format (SLDASM) was compatible with the Stratasys GrabCAD print™ software of the Stratasys J750™ multi-material printer where print mode, orientation, and materials were set. The workflow illustrated in Figure 1. shows the different file formats used in this study. The printing materials selection has been integrated according to the results of the mechanical characterization. The format extensions and file names are associated with a software application, which opens, manages, and saves these types of files used in this study. These are shown in Table 1.

Table 1: 3D File formats used in the current study. Extensions, file names, and software applications.

Format extension	Filename	Software application

(.3dm)	3D Object	Rhinoceros 3D
(.mxp)	Project	Materialise 3-Matic
(.SLDPRT)	3D Object	SolidWorks
(.SLDASM)	Assembly	SolidWorks
(.print)	Print project	GrabCAD Print
(.STL)	Standard triangle language	Global CAD software

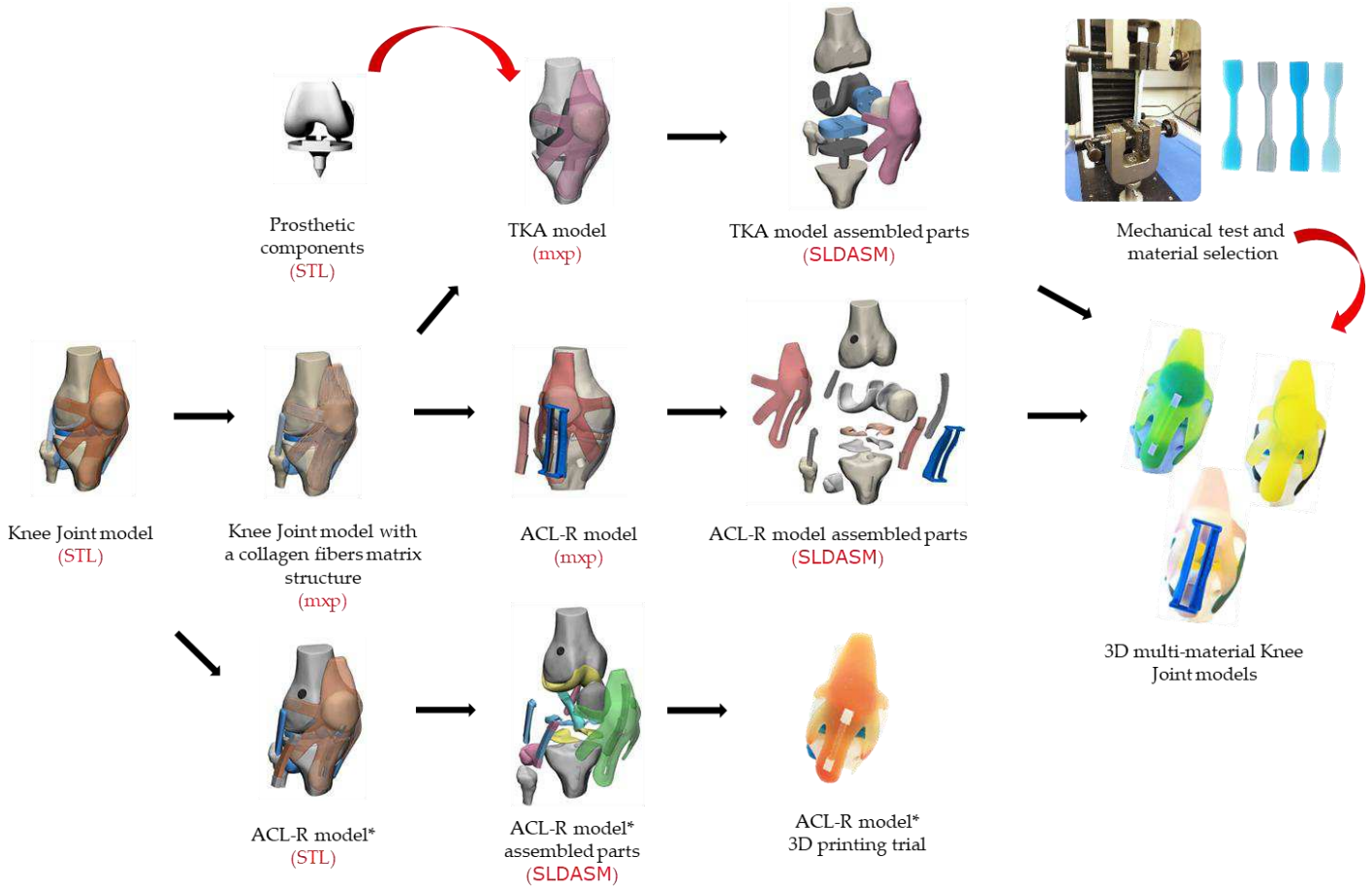

Figure 1: Schematic illustration of the formats used in this study. From the Knee Joint model, three approaches are followed: (1) Design of a collagen fibers matrix that mimics the hierarchical structure of specialized connective soft tissues, (2) development of an ACL-R model integrating key surgical outcomes of the ACL-R computational framework and a custom-made surgical guide (SG) for avoiding graft tunnel length mismatch, and (3) development of a model that represents total joint arthroplasty with the integration of PSP components. The illustration shows a path corresponding to the 3D printing trial with the ACL-R model* used in the previous study.

Knee Joint model manufacturing with a collagen fibers matrix structure.

Knee Joint specialized connective soft tissues play a crucial role, providing strength, transmitting mechanical loads, and contributing to passive support and stability. Indeed, all these functions are made possible by their hierarchical organization. In particular, tendons and ligaments share many similar features. They are load-bearing structures, their high tensile strength ~100-140 MPa and their stiffness ~1.0-1.5 GPa provide all the functional requirements associated with locomotor movement. As expected, both easily bend and change shape to accommodate changes in joint position and skeletal orientation (40).

Highly paralleled collagen fibrous units characterize tendons and ligaments. Accordingly, it can be argued that these tissues are analogous to engineering fiber composites where fibers are laid down in parallel for directional reinforcement (41). The matrix of collagen fibrils aligned (approximate diameter Ø collagen fibril 1.5 nm) is organized into long cross-striated fibrils that are arranged in bundles to form fibers (approximate diameter Ø fiber 50-500 nm). Fibers are further grouped in arrays called fascicles (Ø fascicle 50-300 μm), these arrays together form the ligament (Ø ligament fiber 0.1-0.5 mm) (42). In the Knee Joint, the hierarchical structure of connective tissues described determines the mechanical behavior. Therefore, the knowledge of its mechanical properties is essential to elucidate behavior and function, as well as for selecting appropriate materials used in surgical reconstructive procedures.

To mimic the collagen fibers matrix structure, the STL files of the initial Knee Joint model were exported to Materialise 3-Matic software. A frequent problem in the 3D objects management is the relative position. In general, there is no match between the global reference system (GRS) of the different applications. The Materialise 3-Matic software integrates orientation tools (translate & rotate) for precise positioning of anatomical components according to anatomical references. The first step in fiber design was to establish the orientation of the Knee Joint about the anatomical and GRS planes of the application.

A diameter of 0.6 mm was selected, based on approximate diameter for the fiber (43). A tolerance of 0.1 mm was provided considering a possible expansion of the material during the printing process. Successively we used a systematic method to generate contours and paths for each fiber distinct from each other. Fibers were created along with each structure from traced paths using commands Soft curve &

Sweet-loft. Final matrix fibers structure involved virtual post-processing using Auto-fix, uniform Remesh, Reduce, Smooth & Wrap commands to clean up and correct surface geometry errors, optimize surface mesh and generate a better-refined surface finish for final 3DP.

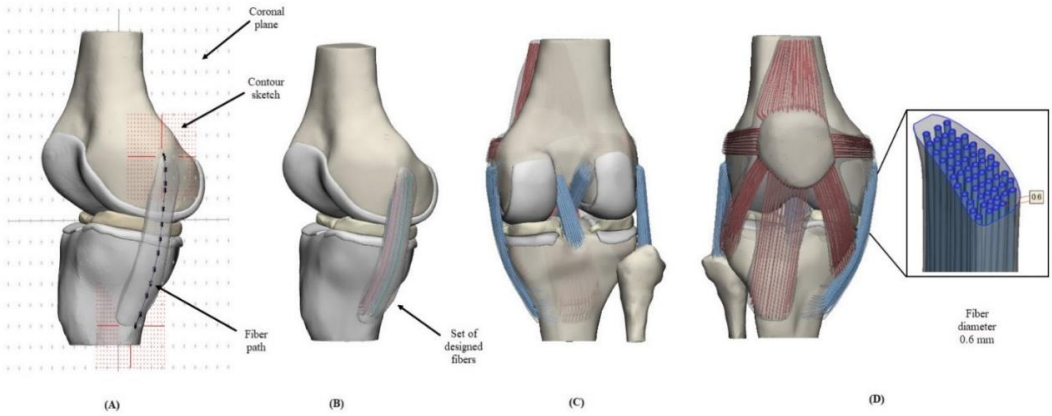

Figure 2: (A) Illustration tracing fibers through the medial collateral ligament (MCL), contour and sketches are shown (B) collagen fibers set manually created to MCL (C) Posterior view of the Knee Joint with all created fibers (D) Anterior view of the Knee Joint, cross-section MCL, the fiber diameter is reported.

The number of designed fibers for cruciate ligaments, collateral ligaments, PT-QT, medial, and lateral patella-femoral ligaments (MPL-LPL), and medial and lateral patellar retinacula (MPR-LPR) were reported in Table 2.

Table 2: Number of fibers designed for the Knee Joint Model.

Soft tissues	Number of fibers
Anterior cruciate ligament (ACL)	50
Posterior cruciate ligament (PCL)	45
Medial collateral ligament (MCL)	60
Lateral collateral ligament (LCL)	50
Quadriceps tendon (QT)	100
Patella tendon (PT)	45
Medial patella-femoral ligament (MPL)	30
Lateral patella-femoral ligament (LPL)	30
Medial patellar retinacula (MPR)	25
Lateral patellar retinacula (LPR)	20

ACL-R model manufacturing and surgical guide for improving surgery outcomes.

The statistics of post-operative clinical outcomes represent the definitive proof of success in the treatment of ligament injuries. It is a clinical basis aimed at improving the results in procedures such as ACL-R. As mentioned, the success of the ACL-R depends on several surgical factors. Various specialists give strong importance to the surgical technique, which is associated with an adequate medical training and accurate pre-operative planning as well as the graft harvest. We sought the manufacture of a multi-material ACL-R model integrating all key surgical outcomes of the ACL-R computational framework using a BPTB auto-graft and a transtibial technique (TT) with single-bundle from a predictive model reported by (34). The approach incorporated orientations-architecture, position-dimensions of the femoral and tibial tunnels as well as the design of a custom-made SG based on the PT anatomy. The SG aimed to solve the problem associated with auto-graft and tunnel length mismatch. Pre-operative measurements of the BPTB auto-graft length were performed, specifically, the distance, measured from the origin in the lower portion of the patella until its insertion in the tibial tubercle. According to (43), if graft length is greater than or equal to 40 mm, the PT graft is a suitable candidate for replacement. Several authors suggest an average length of 40 mm for graft and 20 mm for each bone plug. The BPTB block must have a rectangular geometry, a width of the graft and the bone plugs (tibial and patellar) can range between 9 and 11 mm, a width of 9 mm was chosen. The ACL-R model was developed in the Materialise 3-Matic software. The measurements and landmarks were made from the Knee Joint Model with Measure & Landmark commands. Besides, we consider for the SG design an oscillating saw blade of 0.8 mm wide instead of a traditional scalpel for the graft harvest. Cut-plans, Boolean tools, marking & extrude commands were involved in the SG design. Lastly, the graft harvest was simulated with Boolean tools & Trim commands following the SG dimensions. Femoral and tibial tunnels of the knee were drilled following the orientations, and dimensions reported by (34) with 10 mm drills.

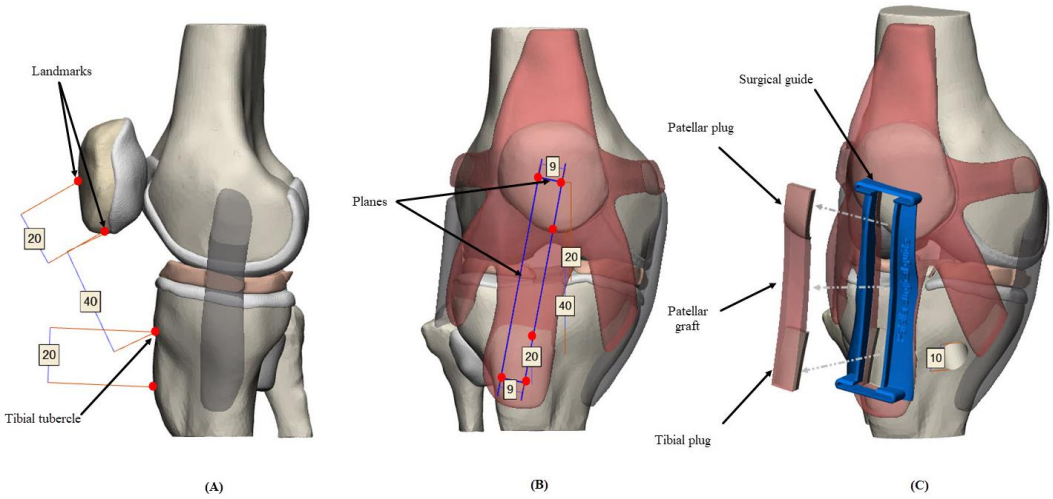

Figure 3: Schematic illustration of the pre-operative measurements and SG positioning. (A) Preliminary measures (mm) and landmarks of BPTB autograft, (B) Simulation of the cut-planes in the graft harvest, (C) Positioned SG, and graft harvest according to the pre-operative guidelines.

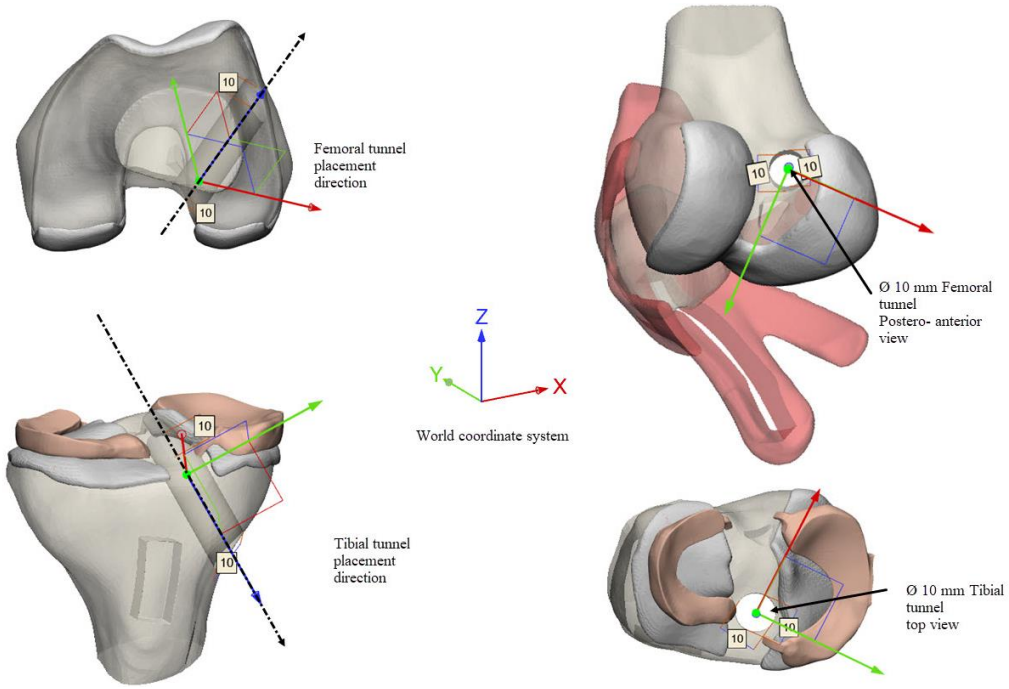

Figure 4: Schematic illustration of the femoral and tibial tunnels architecture, orientations, dimensions, and positions.

TKA model manufacturing and adjustment of PSP components in the Knee Joint model.

TKA involves three critical components: femoral, tibial, and articular components. The femoral component is perhaps the most complex of them. The component has a convex shape, which emulates the curvatures of the femoral condyles (located at

distal femur). The most common cause for premature failure of TKA is aseptic loosening of articular components. When that occurs, all components fail. The wrong relation between implant surfaces is usually the main cause of aseptic loosening. This causes an uneven stress distribution, which leads the component to the failure.

The multi-material TKA model was developed in the Materialise 3-Matic software, the Knee Joint model affected by advanced OA stage with soft tissue involvement was simulated. We chose a custom-made CS implant with symmetric tibial bearing fixed design. The model represents the adaptation and suitable relationship of the prosthetic elements following the requirements: (1) the prosthetic components must have the ability to replicate joint motion as closely as possible. (2) The size of the implants must be custom-made to the actual anatomy of the Knee Joint.

First, the anatomical and mechanical axes of the bone components were defined. Pre-operative measurements of the clinical angles were performed using Measure & Landmark commands: anatomic-mechanic femoral angle (FMAa) anatomic lateral distal femoral angle (FDLAa) and mechanical lateral distal femoral angle (FDLMa) (44). Likewise, measurements of the bone components were performed for the custom-made design of the prosthetic components. Cutting Planes & Trim commands were used to remove bone and cartilage components as follows: 11 mm of the proximal tibia (cross-section), 8 mm of the distal femur (cross-section), 7 mm in the posterior region of the femur (coronal section), 11 mm in the postero-inferior region of the femur (cross-section) and 6 mm in the anterior region of the femur (coronal section), ensuring a space of 20 mm for the replacement of the joint component. The patella was resected 14 mm from the anterior region (coronal section).

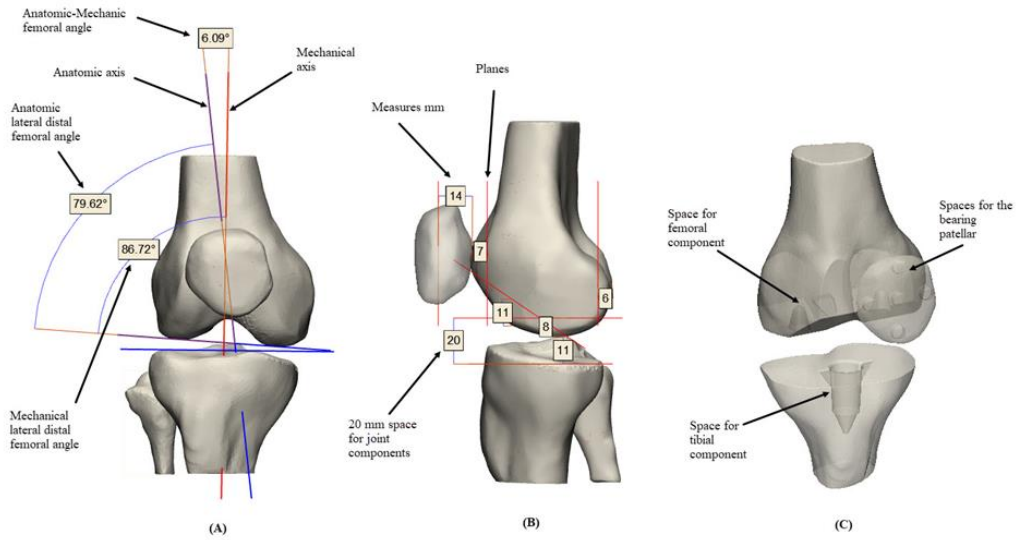

Figure 5: Schematic illustration of the pre-operative measurements and simulated cutting planes. (A) Mechanical and anatomical angles FMAa = 6.09º [5-7º] -FDLAa = 79.62º [79-83º] -FDLMa = 86.72º [85-90º] with their normal angular ranges were reported, (B) Anatomical measurements and simulation of the cutting planes in the bone components, (C) subtraction of the prosthetic components of the bone component according to the planes.

The femoral and tibial components were exported from Rhinoceros 3D (Robert McNeel & Associates) where they were designed based on bone measurements through standard, Planes & Set View commands (Figure 6). The implants were adapted to the bone components, the tibial and patellar bearings were designed from them using Boolean & Marking commands. These were adapted to the trajectory and geometry of the femoral and tibial components respectively. In the neutral position, the femoral component was aligned, so that the resection of the distal bone was perpendicular to the mechanical axis of the femur, and the anterior and posterior resections are parallel to each other (Figure 7).

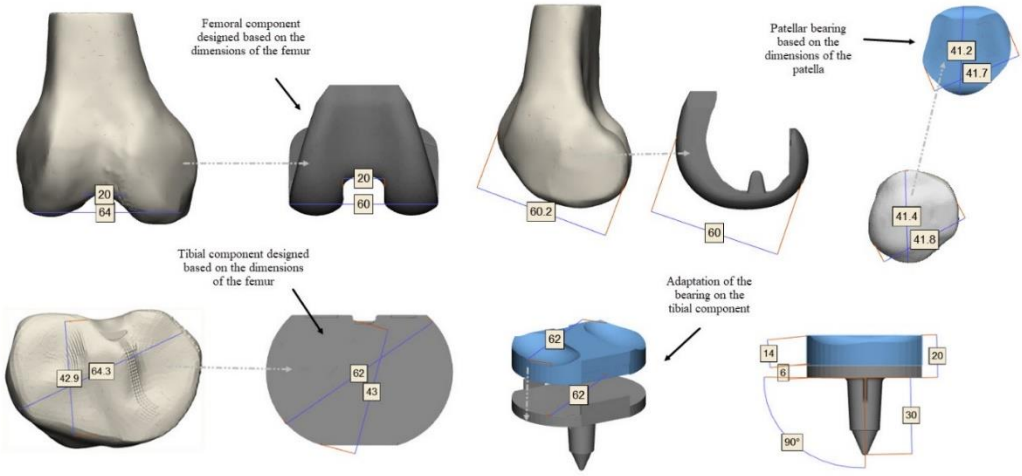

Figure 6: Schematic illustration of the prosthetic components adjustment. Design components were based on the anatomy of the bone components. Patellar and tibial bearings were designed based on the femoral component.

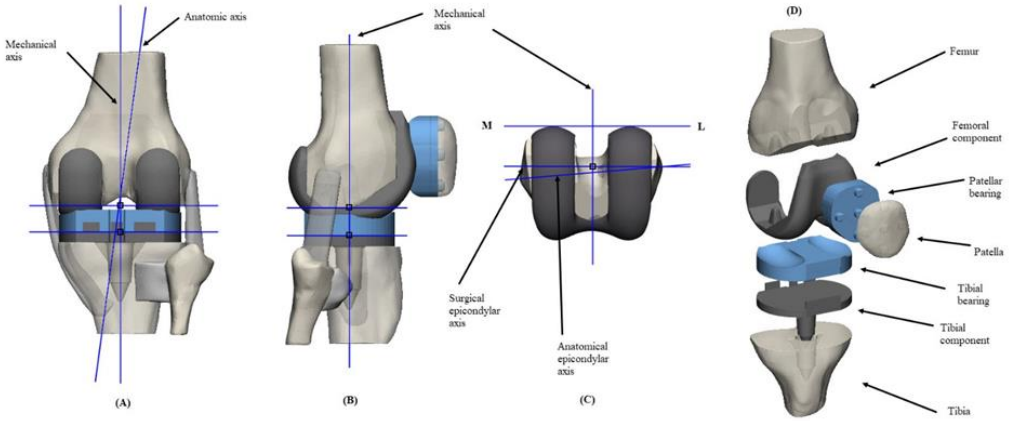

Figure 7: Schematic illustration of the TKA model alignment in a neutral position. (A) Posterior view TKA model, femoral and tibial components are aligned perpendicular to the mechanical axis. (B) Lateral TKA model, the alignment corresponded to 90° concerning the mechanical axis. (C) Transverse view TKA model, the femoral component, anatomic axes-alignment surgical epicondylar axis, and mechanical axis corresponded to 90°. (D) Isometric view assembly of all the components of the TKA model.

Mechanical test and the Material selection and matching.

To print the proposed PSAMs, a key aspect was to determine appropriate material to emulate real tissue mechanical properties. Therefore, our first approach was to explore printer Stratasys J750™ multi-material capabilities. A matching between shore A hardness scale values of printing available materials and Knee Joint

anatomical structures were made. A model of ACL-R proposed in the previous study without considering the designed fiber matrix was printed after materials matching (Table 3). The materials Digital ABS™, Agilus30™, and Tango: FLX950™-FLX930™ (rubber-like materials family) were selected for printing bone components and soft tissues respectively. High Mix 27µm layer thickness mode was set for the model printing.

Table 3: Proposed material matching.

Model Structures	Materials selected	Durometer selected (Shore A)
Bones	Digital ABS™	A 95
Ligaments	Agilus30 FLX2040™	A 35
Tendons	Agilus30 FLX2040™	A 35
Retinacula	Agilus30 FLX2040™	A 30
Menisci	TangoGrayFLX950™	A 75
Cartilage	TangoFLX930™	A 28

Unfortunately, the printing trial was not satisfactory, ligaments and tendons failed easily after simulating flexo-extension movements (Figure 8.)

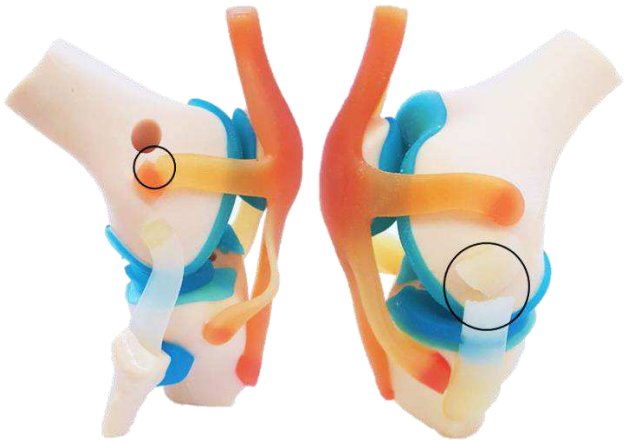

Figure 8: Printing trial scale 1:2. ACL-R model without collagen fibers matrix structure. Knee Joint lateral views in flexion with BPTB graft replacing ACL, rupture of the LPL, and MCL.

After examining the results of the first printing trial, for the printing materials selection of the proposed models, we took advantage of the Stratasys J750 ™ printer's capability. Different combinations of hardness values of fibers were proposed. All models are based on the Knee Joint model. The Mechanical

characterization of the proposed combinations was conducted in Northwestern University Kaiser Lab using an Instron S3300 (Canton, MA) uniaxial testing instrument, following test designation D412-C for rubbers and elastomers. To perform the uniaxial tensile tests, it was necessary to design bone specimens with fibers inside (Table 4), in SolidWorks software following standard specifications (Figure 9.). Three bone specimens (n=3) were printed for each combination. Dimensions (thickness, length, width) of each bone specimen were measured with calibrator, values were set in the software BlueHill, Instrom SA (France, Elancourt). The tensile test was set using a test speed of 10 mm/min. Each bone specimen was attached between the materials testing system extensometer grips to apply tensile loads. The test was performed until the bone specimen failed. Data was recorded and exported to Microsoft Excel. The procedure was repeated with all bone specimens. Strain-stress curves of each specimen were elaborated in Matlab (MathWorks R2018). From them, average curves were created for each combination, elastic modulus, yield strength, and proportional limit values were reported in the results section.

Table 4: Fibers-specimen hardness combinations (Agilus30) for the tensile test.

Material combinations	Fibers Durometer (Shore A)	Specimen Durometer (Shore A)
No 1	A.50	A60
No 2	A.50	A55
No 3	A.50	A40
No 4	A.60	A70

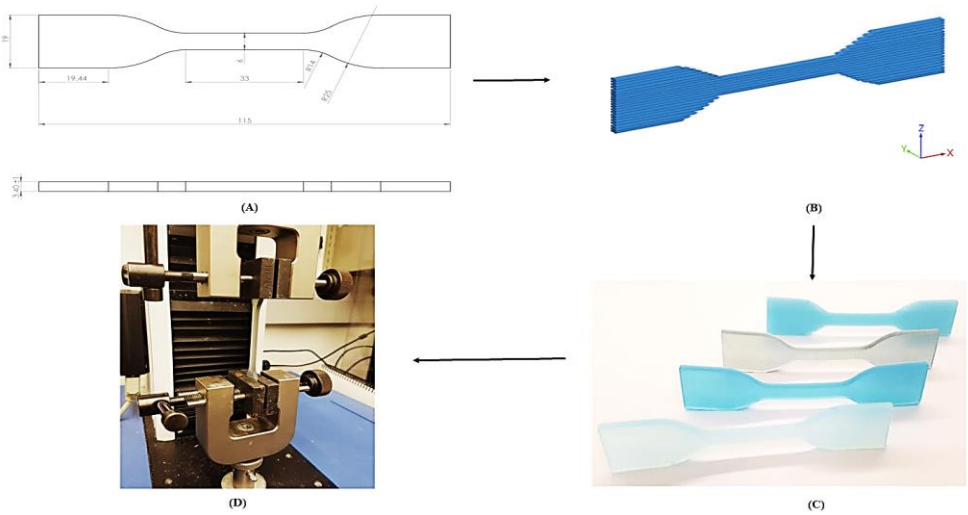

Figure 9: Flowchart application standard D412-C. (A) Dimensions bone specimen (mm), (B) Render bone specimen in SolidWorks software, (C) Printed bone samples with different combinations, (D) Bone specimen attached to a materials testing system Instron S3300 uni-axial testing instrument, to apply tensile load.

Results

Mechanical test.

The tensile test was performed to make a stiffness comparison (directly related to the slope of the linear region) of the different material combinations and Knee Joint soft tissues. We performed three mechanical tests for each combination to obtain average values reported. The approximate elastic modulus and linear tendencies were calculated in the elastic region (a linear approximation from endpoints of the toe-region to the yield strength point) of the stress-strain curves. The Table 5. includes values of Average-standard deviation of proportional limit (AVG/STD-PL), Average-standard deviation of yield strength (AVG/STD-YS), Average-standard deviation of elastic modulus (AVG/STD-E) and linear adjustment coefficient or Pearson's correlation coefficient R^2, which varies between 0.980-0.991.

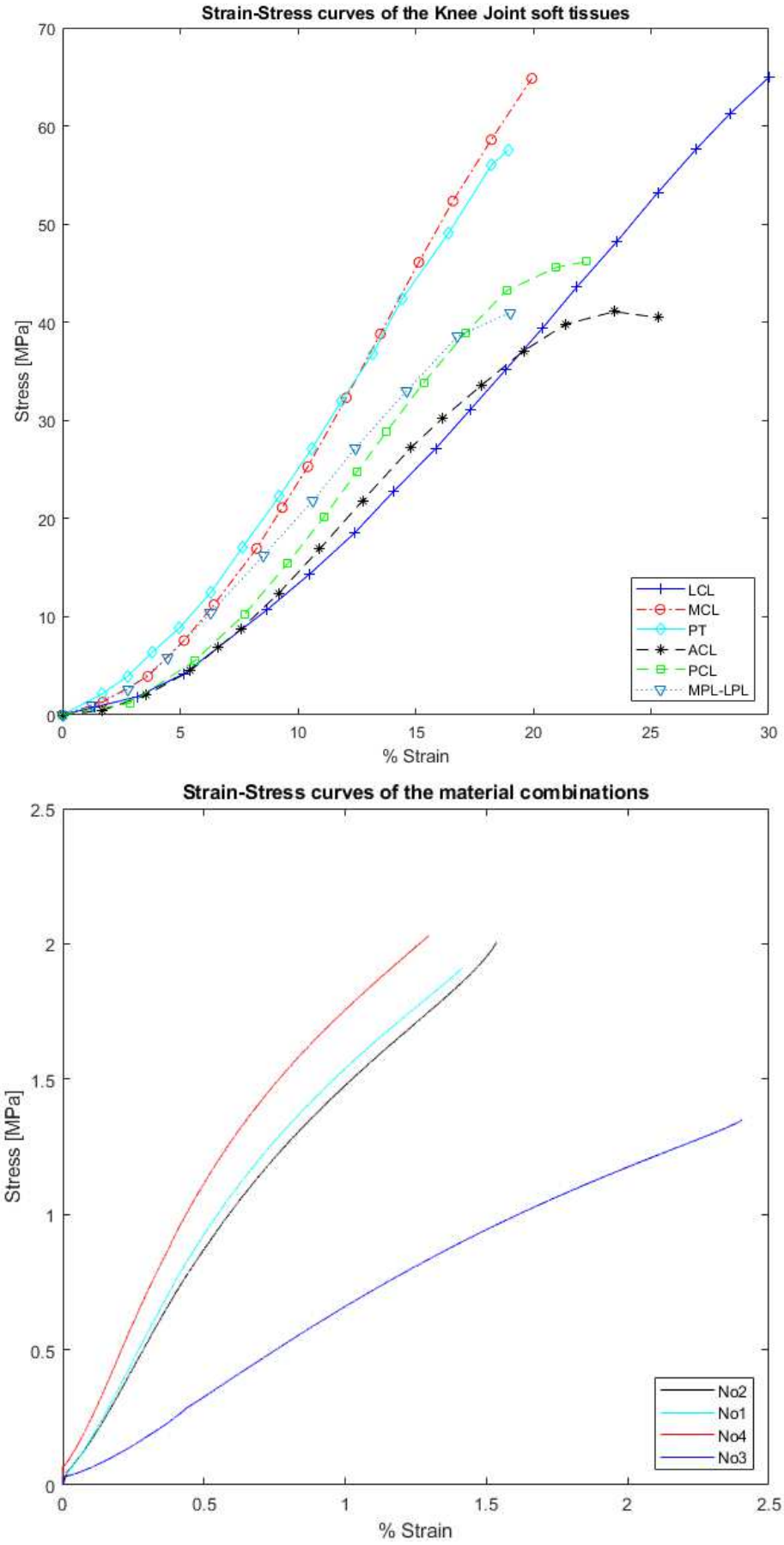

Figure 10: Experimental average Stress-Strain curves of the Knee Joint soft tissues and material combinations.

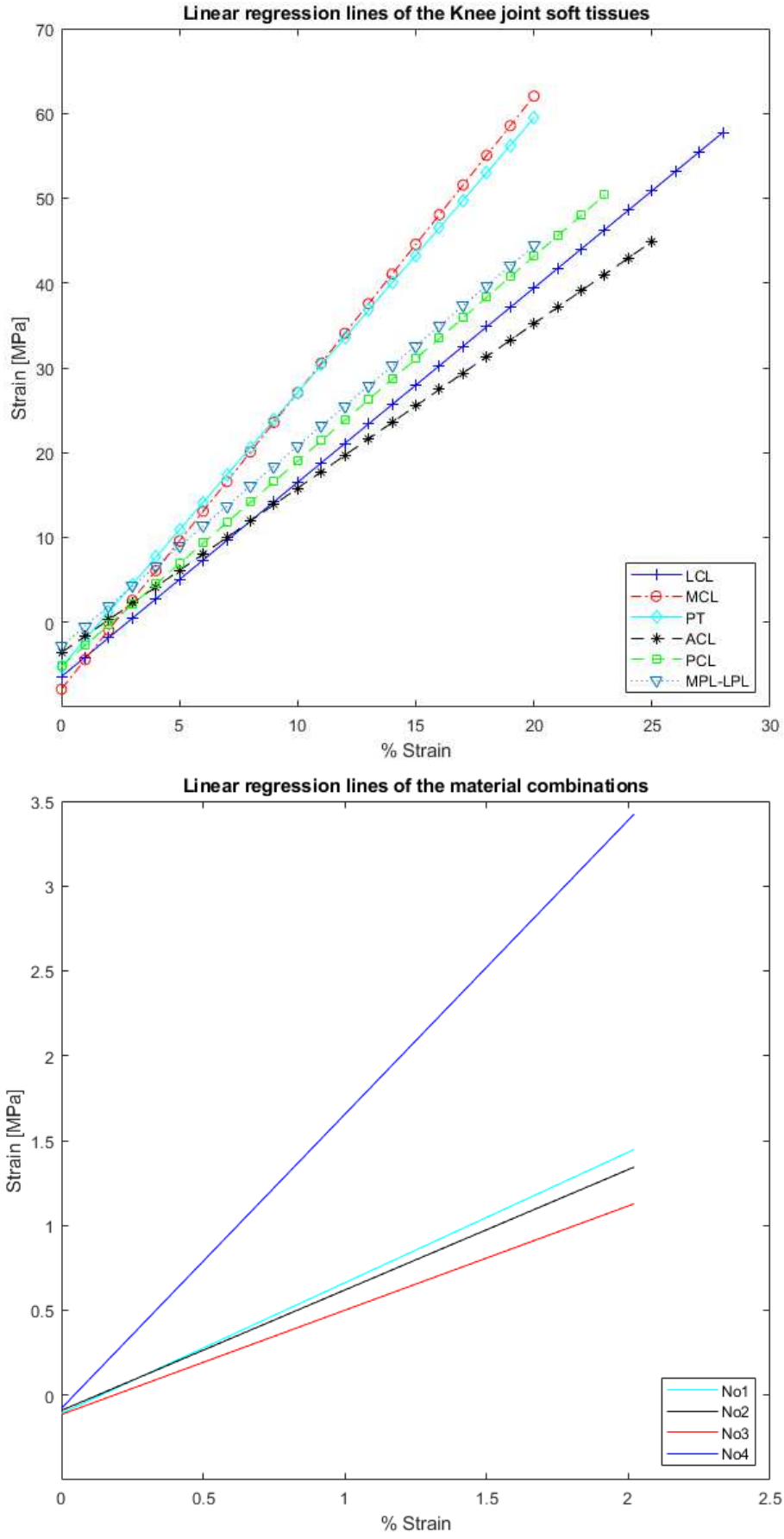

Figure 11: Average linear tendencies for Knee Joint soft tissues and material combinations.

Table 5: Tensile test data. Strain-stress curve properties of different printing materials combinations.

Material combinations	AVG-PL (MPa)	STD-PL	AVG-YS (MPa)	STD-YS	AVG-E (MPa)	STD-E	R^2
No 1	1.533	0.030	1.560	0.008	0.769	0.011	0.980
No 2	1.436	0.035	1.516	0.034	0.751	0.009	0.975
No 3	1.486	0.012	1.580	0.008	0.660	0.005	0.970
No 4	2.336	0.016	2.426	0.002	1.822	0.003	0.991

We compared soft tissue curves (45) with the curves obtained from different proposed combinations; both show the same mechanical pattern exhibiting an approximate linear behavior (Figure 11). When we were comparing the stiffness and elastic modulus values, we found that combinations No 1-4 were the most similar to real structures with elastic modules of 1.8 and 0.7 respectively (Table 6).

Table 6: Matching of the soft tissues with the selected combinations for the PSAMs models.

Knee Joint soft tissues	Elastic modulus (MPa)	Selected combination	Elastic modulus (MPa)
MCL	3.23	No 4	1.8
PT-QT	3.5	No 4	1.8
MPL-LPL	2.41	No 1	0.76
PCL	2.36	No 1	0.76
LCL	2.29	No 1	0.76
ACL	1.93	No 1	0.76

Agilus30: FLX2040™ printing materials in the combinations No 1 (A50 fibers and A60 body) - 4 (A60 fibers and A70 body) were chosen to print ligaments, tendons, and retinacula according to the matching. Tango FLX930™ (A28) - FLX950™ (A75) printing materials were chosen to print cartilage surfaces and menisci respectively. Finally, Digital ABS™ (A95) was chosen to print bone components.

3D Printing of the Patient-specific anatomical models.

Three patient-specific Knee Joint models ACL-R preview study (34), ACL-R, and TKA were printed. The models produced were accurate with no difference in size and positioning relative to planed 3D computer-generated PSAMs replicating fibers and realistic features of the Knee Joint anatomy. In this study, we did not evaluate the anisotropy of PolyJet AM technology (two critical factors involved orientation and LT). We have set PSAMs printing using High Mix six different materials (0.027mm LT) mode according to factory default settings. We located the model perpendicular to the printing tray in which, Z-axis of the SolidWorks GRS coincides with the Z-axis of the printing tray. The multi-material 3D printing enabled the combination of hard and elastic materials in a single project, enabling the 3D printing of the hierarchical structure, custom-made SG, and PSP for TKA. After the completion of printing, wax-like support material was removed using a pressure water gun, the whole process took about 5 minutes. One of the advantages of the use of PolyJet AM technology is the easy support material removal. Indeed, other technologies such as FDM use soluble plastics in chemical baths at high temperatures as a method of remove support material. The removal process can take approximately a day or more, which extends the manufacturing chain. In general, the printing price of PSAMs could be considered profitable about the costs associated with the use of cadaver models or traditional educational models. This was USD 570 with a production time of 28 hours. Finally, it was possible to validate the collagen fibers matrix structure designed and material proposed combinations in the models. After removing support material, the PSAMs were evaluated manually simulating 50 flexo-extension cycles using a three-in-one multi-purpose oil (ACL-R model was tested without BPTB positioned). The PSAMs did not present rupture or wear in their connective structures or at the insertion points. The custom-made SG matches perfectly with the anatomy of the PT in the ACL-R model. Likewise, as it was planned, the BPTB measurements match perfectly with the SG dimensions. The custom-made implants of the TKA model accomplished its requirements and established preliminary planning but the range of motion was more limited.

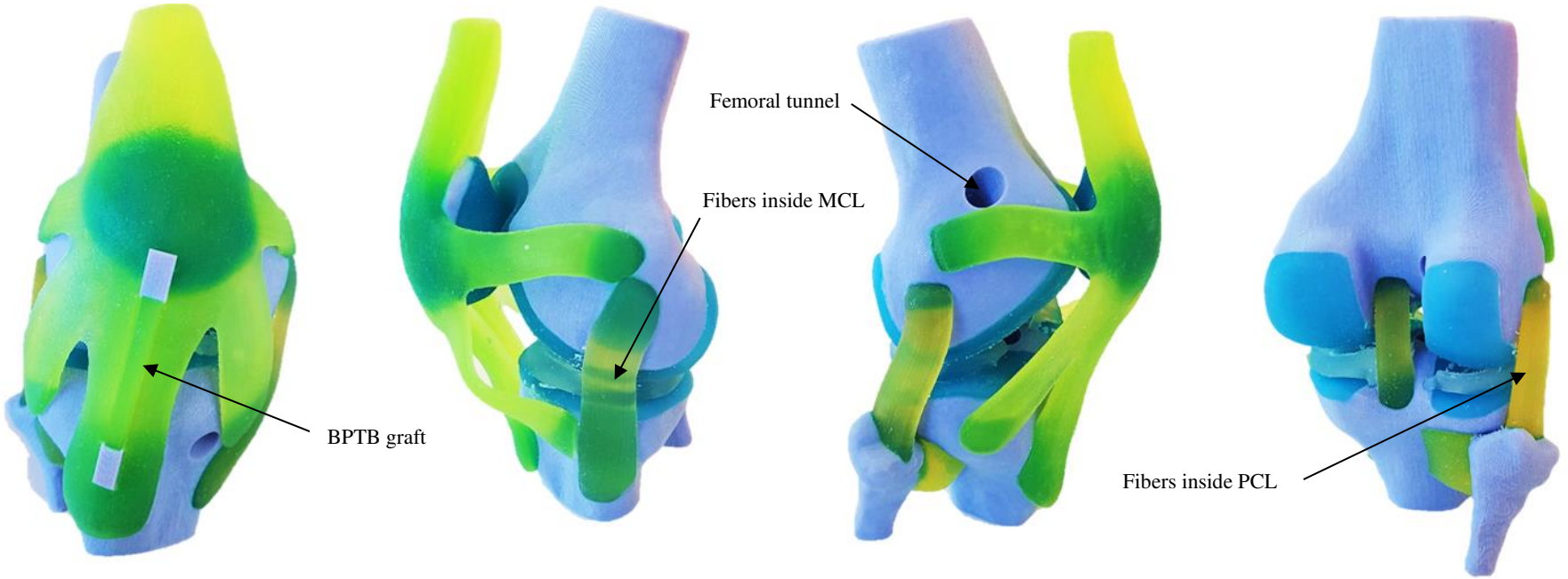
BPTB graft
Fibers inside MCL
Femoral tunnel
Fibers inside PCL

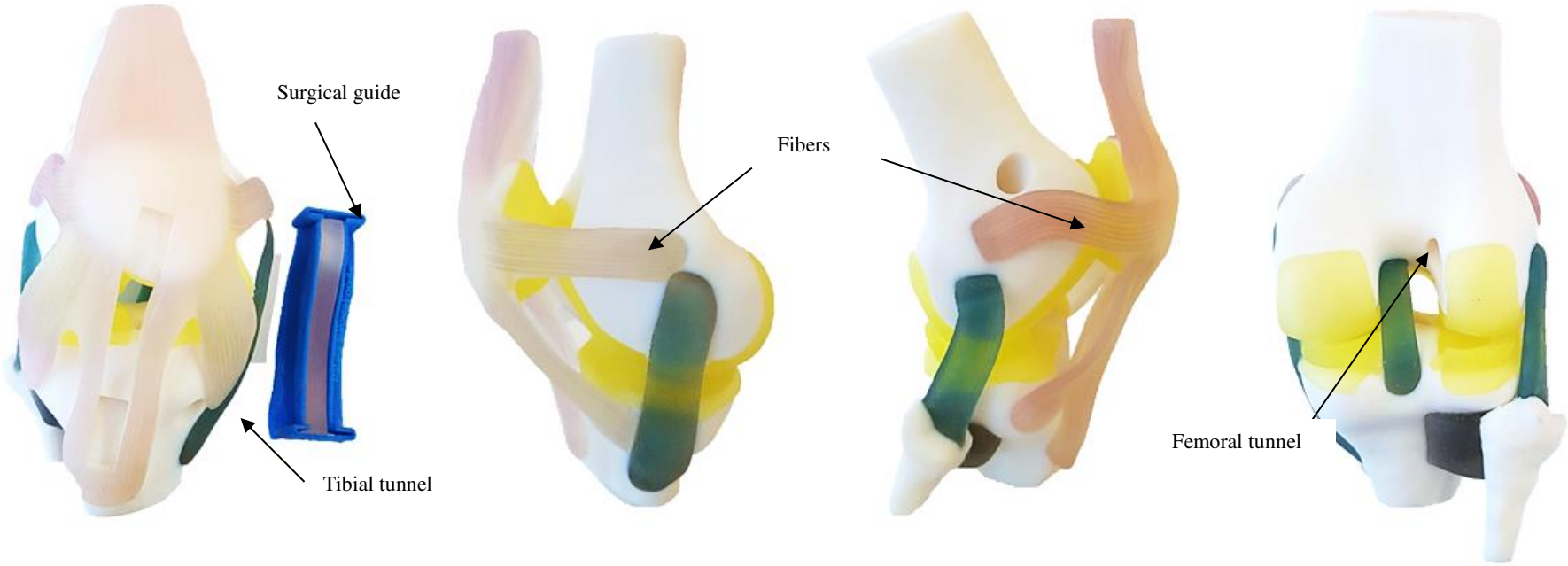
Surgical guide
Tibial tunnel
Fibers
Femoral tunnel

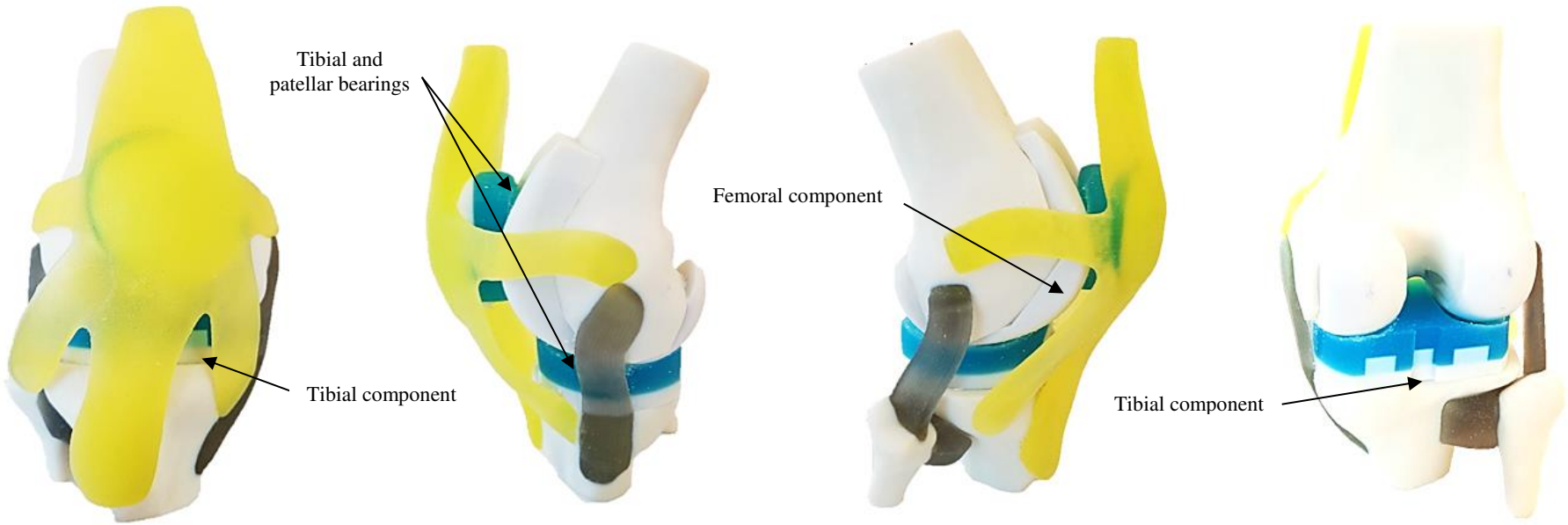

Figure 12: Illustration of Knee Joint PSAMs: (1) Anterior-Lateral- Posterior views of ACL-R (preview study), (2) ACL-R, and (3)TKA models. Final models showed the same details as the 3D computer-generated PSAMs, where the fibers were evident in the grafts and other anatomical structures.

Discussion

The aim of the current study was to take advantage of the multi-color and multi-material Stratasys J750™, and to use CAD software to mimic anatomical features of the soft tissue structures. In addition, the SG and PSP were designed to improve surgical outcomes in orthopedics, particularly in ACL-R as well as providing functional models for TKA. We concluded that the approach mimicking the hierarchical structure of the Knee Joint connective soft tissues was successful. When we compared Stress-Strain curves for Knee Joint soft tissues and material combinations as well as linear tendencies (Figures 10-11), we highlighted that mechanical patterns and stiffness are comparable, despite different elastic modulus values. For the proposed combinations, Pearson correlation coefficients R^2, were close to one, which means that data adjustment was a good approximation of the linear region, representative of the elastic behavior of ligaments and tendons (Table 6). From a functional point of view, when we compared the initial ACL-R model (without hierarchical structure) and ACL-R proposed model, we confirmed that the last one achieved expected results without connective structures wear or rupture. In general, the proposed PSAMs withstood repetitive flexo-extension cycles without problems (Figure 12).

The custom-made ACL printed surgical guide matches perfectly with the anatomy of the PT in the ACL-R model. This would enable the surgeon to solve the problem related to graft tunnel length mismatch and uncertainty in the graft harvest, ensuring dimensions established in the pre-operative plan. The main limitation of this approach is surgical validation, it is expected that the SG can be used in the application of real cases of ACL-R. Figure 13. Shows the comparison between the traditional approach and the proposed solution.

Figure 13: Traditional approach for BPTB autograft harvest using a ruler to measure graft dimension and proposed approach using ACL surgical guide.

Finally, in our study, the purpose of the TKA model was to fulfill the functional requirements established in preoperative planning. There were two main limitations: the PSP designed considered an extreme case of OA in which the cruciate ligaments are sacrificed, which is not recommended from the medical criteria. Besides, the approach was based on a Knee joint under normal conditions and it does not represent a real OA condition, therefore despite the results, the PSP designed are not a real application for TKA. Other critical factors determine the success or failure of TKA that this study does not consider.

Our study serves as the first step and a proof of concept for the accurate creation of PSAMs, SG, and PSP.

Conclusion

The full-color, multi-material 3D printer: Stratasys J750™ has demonstrated its capability to produce functional PSAMs with high fidelity, cost, and short-duration from planning to manufacturing. The proposed PSAMs offer a diverse range of applications. These can be considered as an alternative to replacing cadaver specimens for medical training, pre-operative planning, research and education purposes, and predictive models validation. We highlight the potential of PolyJet AM technology combined with specialized medical software as a path to change the way specialists and researchers plan, execute, and validate complex procedures.

Abbreviations

AM: additive manufacturing, 3DP: three-dimensional printing, PSAMs: Patient-specific anatomical models, DICOM: digital imaging and communications in medicine, CT: computed tomography, MRI: magnetic resonance imaging, US: ultrasound, CAD: computer-aided design, CAE: computer-aided engineering , TKA: total knee arthroplasty, PSP: patient-specific prostheses, PSI: patient-specific instrumentation, ACL: anterior cruciate ligament, ACL-R: anterior cruciate ligament reconstruction, SG: surgical guide OA: osteoarthritis, BPTB: bone-patellar tendon-bone, STG: semitendinosus-gracilis, CS: cruciate sacrificing, UV: ultraviolet, LT: layer thickness, ABS: acrylonitrile butadiene styrene, FDM: Fused Deposition Modeling, STL: standard triangle language, PF: patello-femoral,

TF: tibio-femoral, PT; patella tendon, QT: quadricep tendon, GRS: global reference system, PCL: posterior cruciate ligament, MCL: medial collateral ligament, LCL: lateral collateral ligament, MPL: medial patella-femoral ligament, LPL: lateral patella-femoral ligament, MPR: medial patellar retinacula, LPR: lateral patellar retinacula, TT: transtibial technique, FMAa: anatomic-mechanic femoral angle, FDLAa: anatomic lateral distal femoral angle, FDLMa: mechanical lateral distal femoral angle, AVG/STD-PL: average-standard deviation of proportional limit, AVG/STD-YS: average-standard deviation of yield strength, AVG/STD-E: average-standard deviation of elastic modulus.

Acknowledgments

We would like to express our sincere gratitude to the Engineer. Eric Renteria, application Engineer at Materialise US. Who provided us a provisional license to try out Mimics innovation suite. The specialized software Materialise 3-Matic research version proved quite useful and versatile. Its measurement, simulation, positioning, meshing, and design tools enabled the development of the proposed models. Likewise, our sincere thanks go to Engineers: Kunal Shah, a research engineer at the Center for Bionic Medicine within the Shirley Ryan AbilityLab and Samuel Sung, a research assistant at Northwestern University KaiserLab who provided me support and access to the laboratories and research facilities. Without their continued support, it would not be possible to conduct this research.

Authors' contributions

The author(s) read and approved the final manuscript.

Authors' information

Not applicable.

Funding

The Shirley Ryan Abilitylab and Northwestern University supported this study.

Availability of data and materials

The 3D computer-generated PSAMs used to support the findings of this study are available from the corresponding author on reasonable request.

Ethics approval and consent to participate

Not applicable.

Consent for publication

Not applicable.

Competing interests

The corresponding authors declare that they have no competing interests related to this study.

References

1. Ashish, Ahmad N, Gopinath P, Vinogradov A. 3D Printing in Medicine In: 3D Printing Technology in Nanomedicine. Elsevier; 2019. p. 1–22. DOI: 10.1016/B978-0-12-815890-6.00001-3
2. Tood P. The impact of implementing 3D Printing at the point-of-care In: Materialise medical. Whitepapers. 2018. https://www.materialise.com/en/resources/medical/whitepapers/impact-of-implementing-3d-printing-at-point-of-care
3. Yan Q, Dong H, Su J, Han J, Song B, Wei Q, et al. A Review of 3D Printing Technology for Medical Applications. Engineering. 2018;4(5):729–42. DOI: 10.1016/j.eng.2018.07.021
4. Anderson PA. 3D Printing for Education and Surgical Planning in Orthopedic Surgery. 3D Printing in Orthopaedic Surgery. Elsevier Inc.; 2019. 55–63 p. DOI: 10.1016/B978-0-323-58118-9.00006-3
5. Bücking TM, Hill ER, Robertson JL, Maneas E, Plumb AA, Nikitichev DI. From medical imaging data to 3D printed anatomical models. PLoS One. 2017;12(5):1–10. DOI: 10.1371/journal.pone.0178540
6. Lal H, Patralekh MK. 3D printing and its applications in orthopaedic trauma: A technological marvel. J Clin Orthop Trauma. 2018;9(3):260–8. DOI: 10.1016/j.jcot.2018.07.022
7. Nadeem M, Jackson E, Rachala SR. 3D Printing in Hip and Knee Arthroplasty. 3D Printing in Orthopaedic Surgery. Elsevier Inc.; 2019. 171–177 p. DOI: 10.1016/B978-0-323-58118-9.00014-2

8. Joskowicz L, Hazan EJ. Computer-aided orthopedic surgery: Incremental shift or paradigm change? Adv Exp Med Biol. 2018;1093:21–30. DOI: 10.1007/978-981-13-1396-7_2

9. Kim JW, Lee Y, Seo J, Park JH, Seo YM, Kim SS, et al. Clinical experience with three-dimensional printing techniques in orthopedic trauma. J Orthop Sci. 2018;23(2):383–8. DOI: 10.1016/j.jos.2017.12.010

10. Vaishya R, Vijay V, Vaish A, Agarwal A. Three-dimensional printing for complex orthopedic cases and trauma: A blessing. Vol. 15, Apollo Medicine. 2018. p. 51–4. DOI: 10.4103/am.am_51_18

11. Kenneth R. Foster. Philosophy and Engineering. In: Michelfelder DP, Newberry B, Zhu Q, editors. Cham: Springer International Publishing; 2017. p. 211–28. DOI: 10.1007/978-3-319-45193-0_16

12. Matsumoto JS, Morris JM, Rose PS. 3-Dimensional printed anatomic models as planning aids in complex oncology surgery. JAMA Oncol. 2016;2(9):1121–2. DOI: 10.1001/jamaoncol.2016.2469

13. Jones GG, Clarke S, Jaere M, Cobb J. 3D printing and unicompartmental knee arthroplasty. EFORT Open Rev. 2018;3(5):248–53. DOI: 10.1302 / 2058-5241.3.180001

14. Qiu B, Liu F, Tang B, Deng B, Liu F, Zhu W, et al. Clinical Study of 3D Imaging and 3D Printing Technique for Patient-Specific Instrumentation in Total Knee Arthroplasty. J Knee Surg. 2017;30(8):822–8. DOI: 10.1055/s-0036-1597980

15. Soni A, Kumar Modi Y, Agrawal S. Computed tomography based 3D modeling and analysis of human knee joint. Mater Today Proc. 2018;5(11):24194–201. DOI: 10.1016/j.matpr.2018.10.214

16. Crawford SN, Waterman BR, Lubowitz JH. Long-term failure of anterior cruciate ligament reconstruction. Arthrosc - J Arthrosc Relat Surg. 2013;29(9):1566–71. DOI: 10.1016/j.arthro.2013.04.014

17. Olsson O, Isacsson A, Englund M, Frobell RB. Epidemiology of intra- and peri-articular structural injuries in traumatic knee joint hemarthrosis – data from 1145 consecutive knees with subacute MRI. Osteoarthr Cartil. 2016;24(11):1890–7. DOI: 10.1016/j.joca.2016.06.006

18. Rankin I, Rehman H, Frame M. 3D-Printed Patient-Specific ACL Femoral Tunnel Guide from MRI. Open Orthop J. 2018;12(1):59–68. DOI: 10.2174/1874325001812010059

19. Ni J, Li D, Mao M, Dang X, Wang K, He J, et al. A Method of Accurate Bone Tunnel Placement for Anterior Cruciate Ligament Reconstruction Based on 3-Dimensional Printing Technology: A Cadaveric Study. Arthrosc - J Arthrosc Relat Surg. 2018;34(2):546–56. DOI: 10.1016/j.arthro.2017.08.288

20. Tisherman R, De Groot J, Rothrauff B, Byrne K, Meredith SJ, Musahl V. The role of anatomic ACL reconstruction in ACL revision surgery. Ann Jt. 2018;3(3):103–103. DOI: 10.21037/aoj.2018.11.14

21. Samuelsson K, Andersson D, Karlsson J. Treatment of Anterior Cruciate Ligament Injuries With Special Reference to Graft Type and Surgical Technique: An Assessment of Randomized Controlled Trials. Arthrosc - J Arthrosc Relat Surg. 2009;25(10):1139–74. DOI: 10.1016/j.arthro.2009.07.021

22. Gans I, Retzky JS, Jones LC, Tanaka MJ. Epidemiology of Recurrent Anterior Cruciate Ligament Injuries in National Collegiate Athletic Association Sports: The Injury Surveillance Program, 2004-2014. Orthop J Sport Med. 2018;6(6):1–7. DOI: 10.1177/2325967118777823

23. Kaeding CC, Pedroza AD, Reinke EK, Huston LJ, Spindler KP, Amendola A, et al. Risk Factors and Predictors of Subsequent ACL Injury in Either Knee After ACL Reconstruction: Prospective Analysis of 2488 Primary ACL Reconstructions from the MOON Cohort. Am J Sports Med. 2015 Jul 21;43(7):1583–90. DOI: 10.1177/0363546515578836

24. Whitehead TS. Failure of Anterior Cruciate Ligament Reconstruction. Clin Sports Med. 2013 Jan;32(1):177–204. DOI: 10.1016/j.csm.2012.08.015

25. Vaishya R, Okwuchukwu MC, Agarwal AK, Vijay V. Does Anterior Cruciate Ligament Reconstruction prevent or initiate Knee Osteoarthritis? -A critical review. J Arthrosc Jt Surg. 2019;6(3):133–6. DOI: 10.1016/j.jajs.2019.07.001

26. Friel NA, Chu CR. The Role of ACL Injury in the Development of Posttraumatic Knee Osteoarthritis. Clin Sports Med. 2013;32(1):1–12. DOI: 10.1016/j.csm.2012.08.017

27. Huang W, Ong TY, Fu SC, Yung SH. Prevalence of patellofemoral joint osteoarthritis after anterior cruciate ligament injury and associated risk factors: A

systematic review. J Orthop Transl. 2020;22:14–25. DOI: 10.1016/j.jot.2019.07.004

28. Van Eck CF, Kropf EJ, Romanowski JR, Lesniak BP, Tranovich MJ, van Dijk CN, et al. ACL graft re-rupture after double-bundle reconstruction: Factors that influence the intra-articular pattern of injury. Knee Surgery, Sport Traumatol Arthrosc. 2011;19(3):340–6. DOI: 10.1007/s00167-010-1297-8

29. Kyritsis P, Bahr R, Landreau P, Miladi R, Witvrouw E. Likelihood of ACL graft rupture: Not meeting six clinical discharge criteria before return to sport is associated with a four times greater risk of rupture. Br J Sports Med. 2016;50(15):946–51. DOI: 10.1136/bjsports-2015-095908

30. Wada O, Gamada K, Aoyama N, Mizuno K, Iwasaki Y. A difference in rotational alignment of the tibio-femoral joint after anterior cruciate ligament reconstruction between the bone-patellar tendon-bone and semitendinosus-gracilis grafts. Clin Biomech. 2019;65:45–50. DOI: 10.1016/j.clinbiomech.2019.03.015

31. Gupta PK, Acharya A, Mourya A, Mahajan P. Comparison of patellar tendon versus hamstrings autografts for anterior cruciate ligament reconstruction in Indian population: A randomised control trial study. J Clin Orthop Trauma. 2019;10(3):581–5. DOI: 10.1016/j.jcot.2018.04.018

32. Duchman KR, Lynch TS, Spindler KP. Graft Selection in Anterior Cruciate Ligament Surgery: Who gets What and Why? Clin Sports Med. 2017;36(1):25–33. DOI: 10.1016/j.csm.2016.08.013

33. Li RT, Lorenz S, Xu Y, Harner CD, Fu FH, Irrgang JJ. Predictors of radiographic knee osteoarthritis after anterior cruciate ligament reconstruction. Am J Sports Med. 2011;39(12):2595–603. DOI: 10.1177/0363546511424720

34. Salehghaffari S, Dhaher YY. A model of articular cruciate ligament reconstructive surgery: A validation construct and computational insights. J Biomech. 2014;47(7):1609–17. DOI: 10.1016/j.jbiomech.2014.03.003

35. Lizaur-Utrilla A, Martinez-Mendez D, Gonzalez-Parreño S, Marco-Gomez L, Miralles Muñoz FA, Lopez-Prats FA. Total Knee Arthroplasty in Patients With Prior Anterior Cruciate Ligament Reconstruction. J Arthroplasty. 2018;33(7):2141–5. DOI: 10.1016/j.arth.2018.02.054

36. Chen D, Shen J, Zhao W, Wang T, Han L, Hamilton JL, et al. Osteoarthritis: Toward a comprehensive understanding of pathological mechanism. Bone Res. 2017;5. DOI: 10.1038/boneres.2016.44

37. Liddle AD, Pegg EC, Pandit H. Knee replacement for osteoarthritis. Maturitas [Internet]. 2013;75(2):131–6. DOI: 10.1016/j.maturitas.2013.03.005

38. Sharkey PF, Hozack WJ, Rothman RH, Shastri S, Jacoby SM. Why are total knee arthroplasties failing today? Clin Orthop Relat Res. 2002;(404):7–13. DOI: 10.1097/00003086-200211000-00003

39. Gay P, Blanco D, Pelayo F, Noriega A, Fernández P. Analysis of Factors Influencing the Mechanical Properties of Flat PolyJet Manufactured Parts. Procedia Eng. 2015;132:70–7. DOI: 10.1016/j.proeng.2015.12.481

40. Biewener AA. Tendons and ligaments: Structure, mechanical behavior and biological function. Collagen Struct Mech. 2008;269–84. DOI: 10.1007/978-0-387-73906-9_10

41. Provenzano PP, Vanderby R. Collagen fibril morphology and organization: Implications for force transmission in ligament and tendon. Matrix Biol. 2006;25(2):71–84. DOI: 10.1016/j.matbio.2005.09.005

42. Hsieh AH, Tsai CM-H, Ma Q-J, Lin T, Banes AJ, Villarreal FJ, et al. Time-dependent increases in type-III collagen gene expression in medial collateral ligament fibroblasts under cyclic strains. J Orthop Res. 2000;18(2):220–7. DOI: 10.1002/jor.1100180209

43. Grawe B, Smerina A, Allen A. Avoiding graft-tunnel length mismatch in anterior cruciate ligament reconstruction: The single-bone plug technique. Arthrosc Tech. 2014;3(3):e417–20. DOI: 10.1016/j.eats.2014.04.003

44. Jingjit W, Poomcharoen P, Limmahakhun S, Klunklin K, Leerapun T, Rojanasthien S. Femoral mechanical-anatomical angle of osteoarthritic knees. J Med Assoc Thail. 2014;97(12):1314–8.

45. Mesfar W, Shirazi-Adl A. Biomechanics of the knee joint in flexion under various quadriceps forces. Knee. 2005;12(6):424–34. DOI: 10.1016/j.knee.2005.03.004

Figures

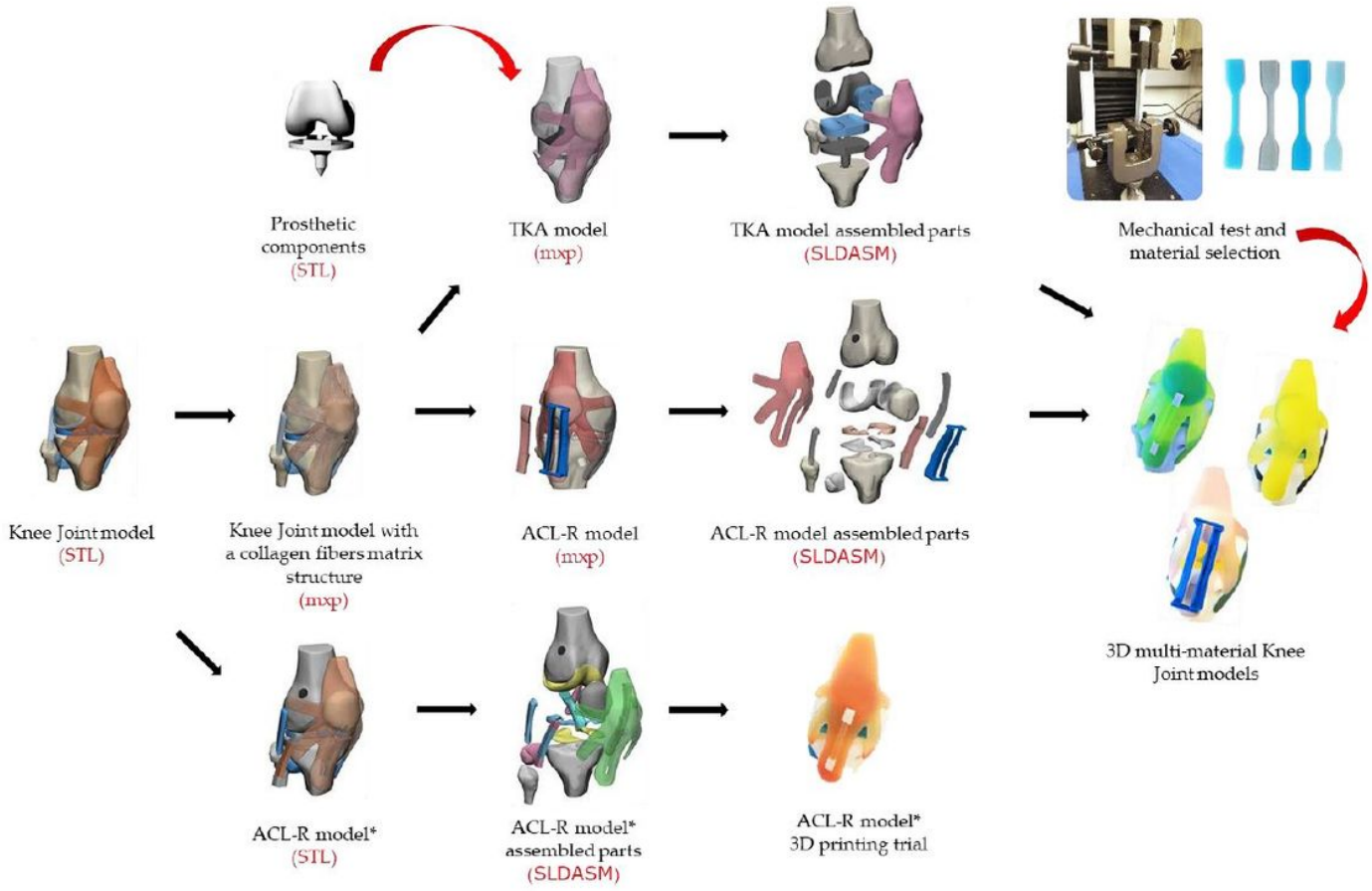

Figure 1

Schematic illustration of the formats used in this study. From the Knee Joint model, three approaches are followed: (1) Design of a collagen fibers matrix that mimics the hierarchical structure of specialized connective soft tissues, (2) development of an ACL-R model integrating key surgical outcomes of the ACL-R computational framework and a custom-made surgical guide (SG) for avoiding graft tunnel length mismatch, and (3) development of a model that represents total joint arthroplasty with the integration of PSP components. The illustration shows a path corresponding to the 3D printing trial with the ACL-R model* used in the previous study.

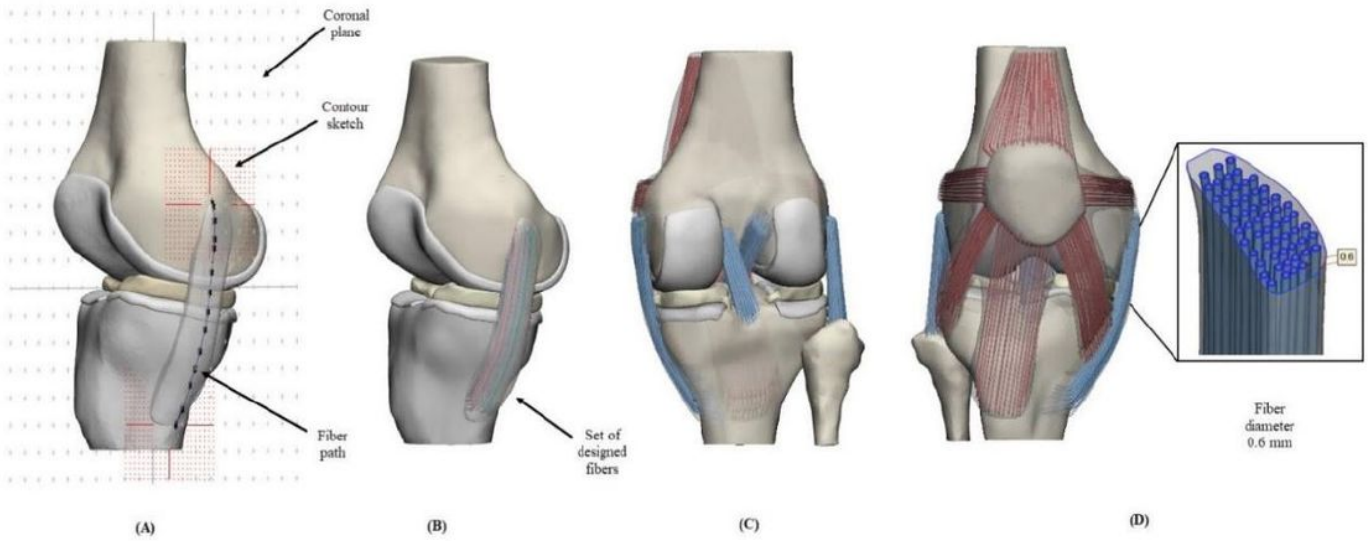

Figure 2

(A) Illustration tracing fibers through the medial collateral ligament (MCL), contour and sketches are shown (B) collagen fibers set manually created to MCL (C) Posterior view of the Knee Joint with all created fibers (D) Anterior view of the Knee Joint, cross-section MCL, the fiber diameter is reported. The number of designed fibers for cruciate ligaments, collateral ligaments, PT-QT, medial, and lateral patella-femoral ligaments (MPL-LPL), and medial and lateral patellar retinacula (MPR-LPR) were reported in Table 2.

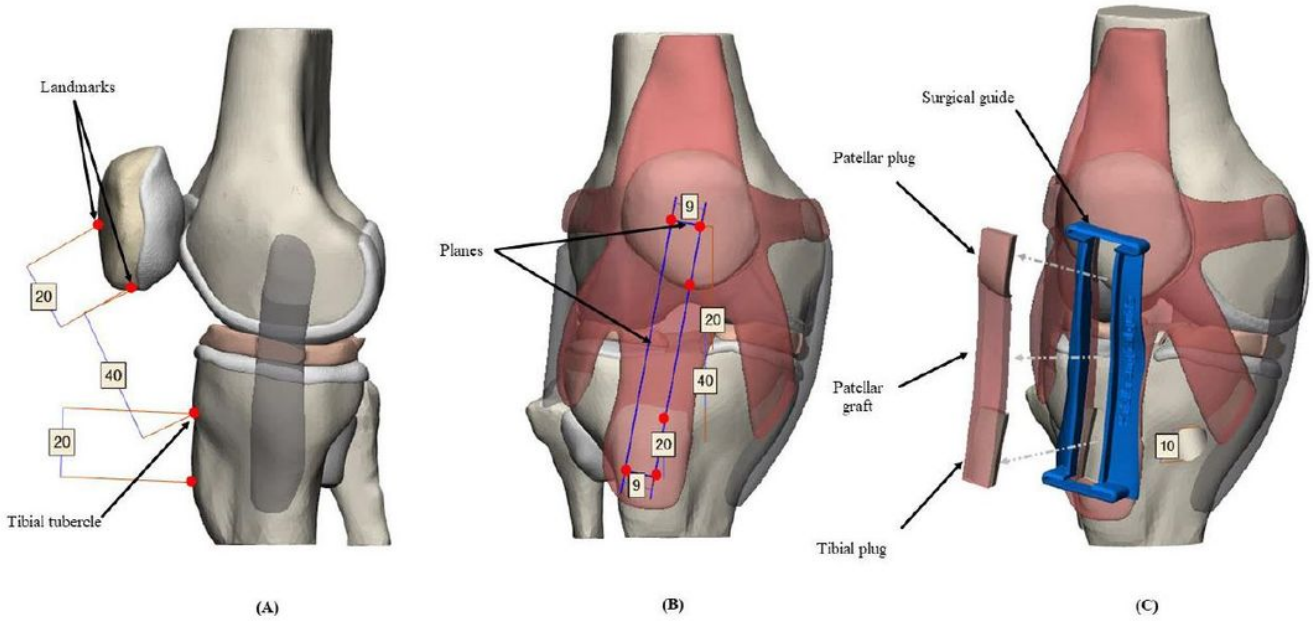

Figure 3

Schematic illustration of the pre-operative measurements and SG positioning. (A) Preliminary measures (mm) and landmarks of BPTB autograft, (B) Simulation of the cut-planes in the graft harvest, (C) Positioned SG, and graft harvest according to the pre-operative guidelines.

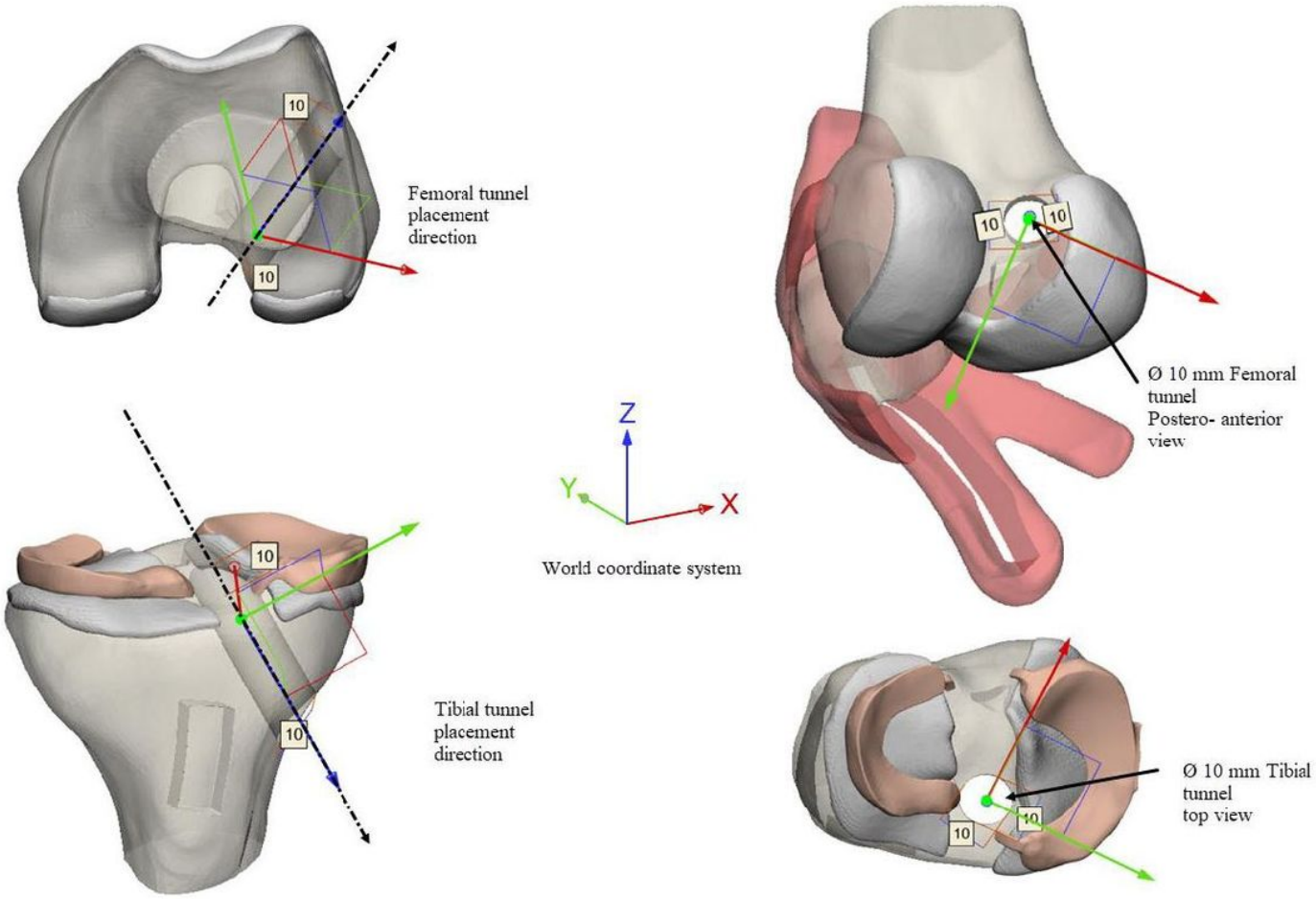

Figure 4

Schematic illustration of the femoral and tibial tunnels architecture, orientations, dimensions, and positions.

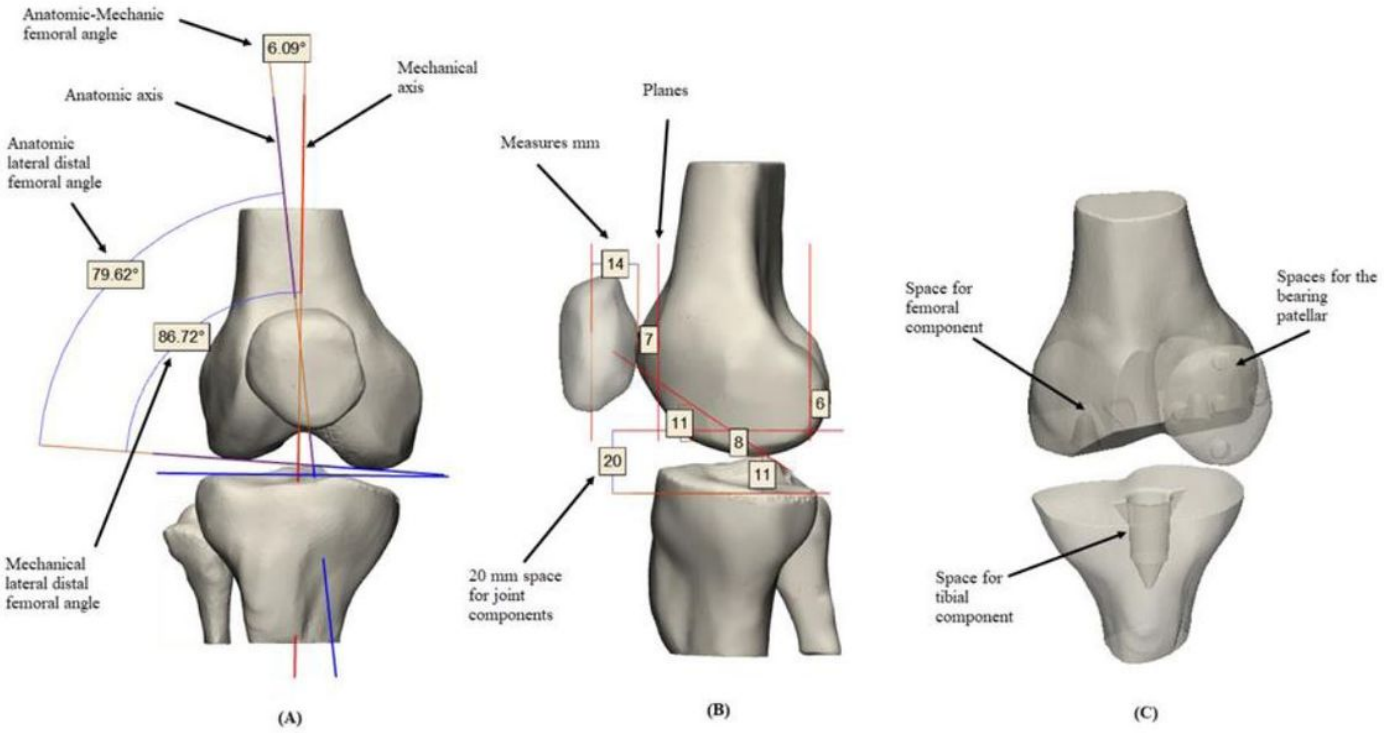

Figure 5

Schematic illustration of the pre-operative measurements and simulated cutting planes. (A) Mechanical and anatomical angles FMAa = 6.09º [5-7º] - FDLAa = 79.62º [79-83º] -FDLMa = 86.72º [85-90º] with their normal angular ranges were reported, (B) Anatomical measurements and simulation of the cutting planes in the bone components, (C) subtraction of the prosthetic components of the bone component according to the planes.

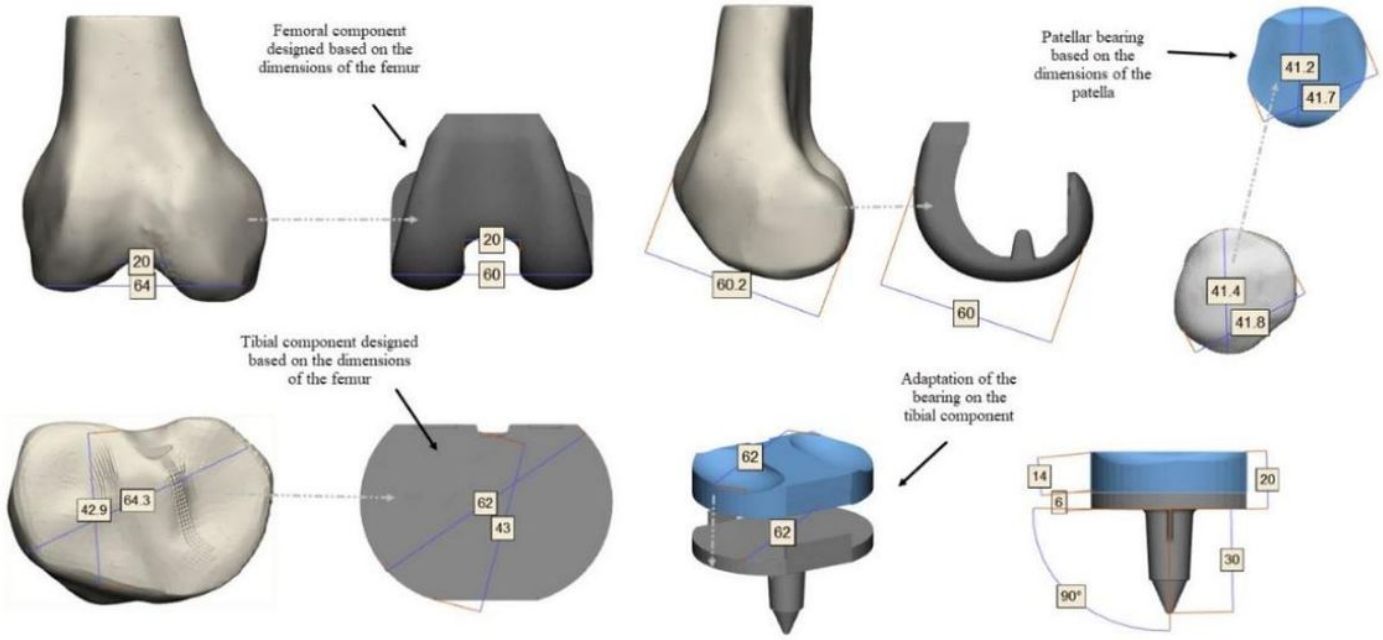

Figure 6

Schematic illustration of the prosthetic components adjustment. Design components were based on the anatomy of the bone components. Patellar and tibial bearings were designed based on the femoral component.

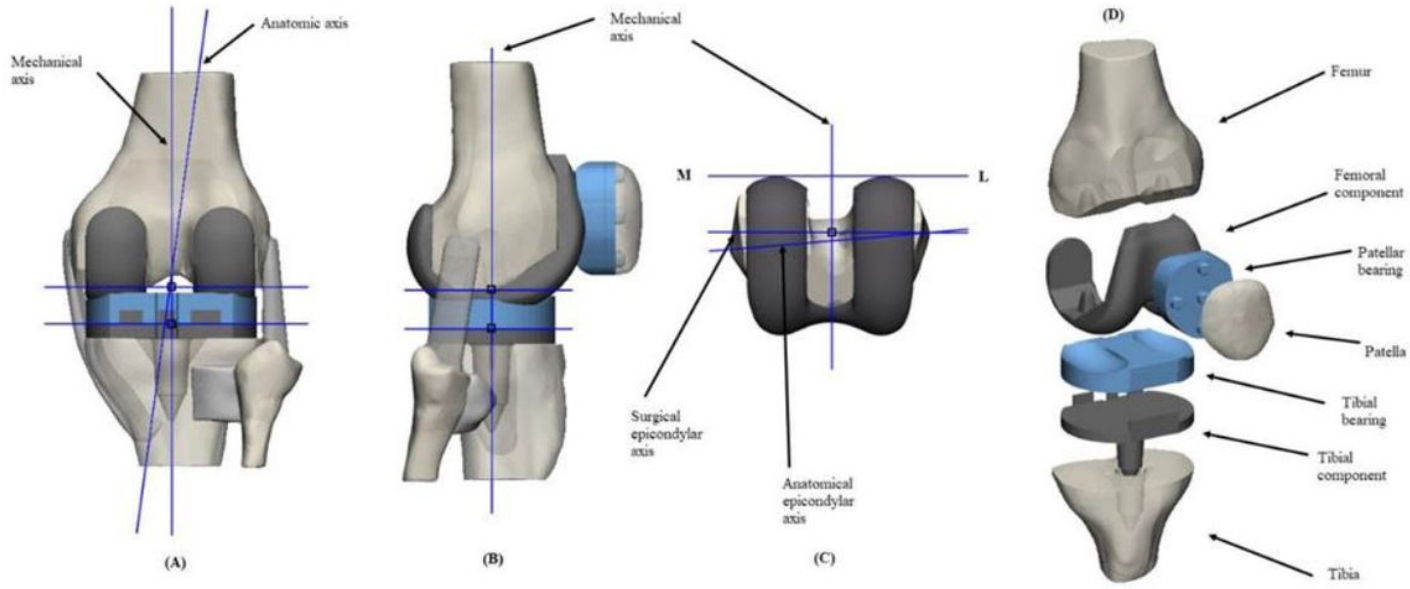

Figure 7

Schematic illustration of the TKA model alignment in a neutral position. (A) Posterior view TKA model, femoral and tibial components are aligned perpendicular to the mechanical axis. (B) Lateral TKA model, the alignment corresponded to 90° concerning the mechanical axis. (C) Transverse view TKA model, the femoral component, anatomic axes-alignment surgical epicondylar axis, and mechanical axis corresponded to 90°. (D) Isometric view assembly of all the components of the TKA model.

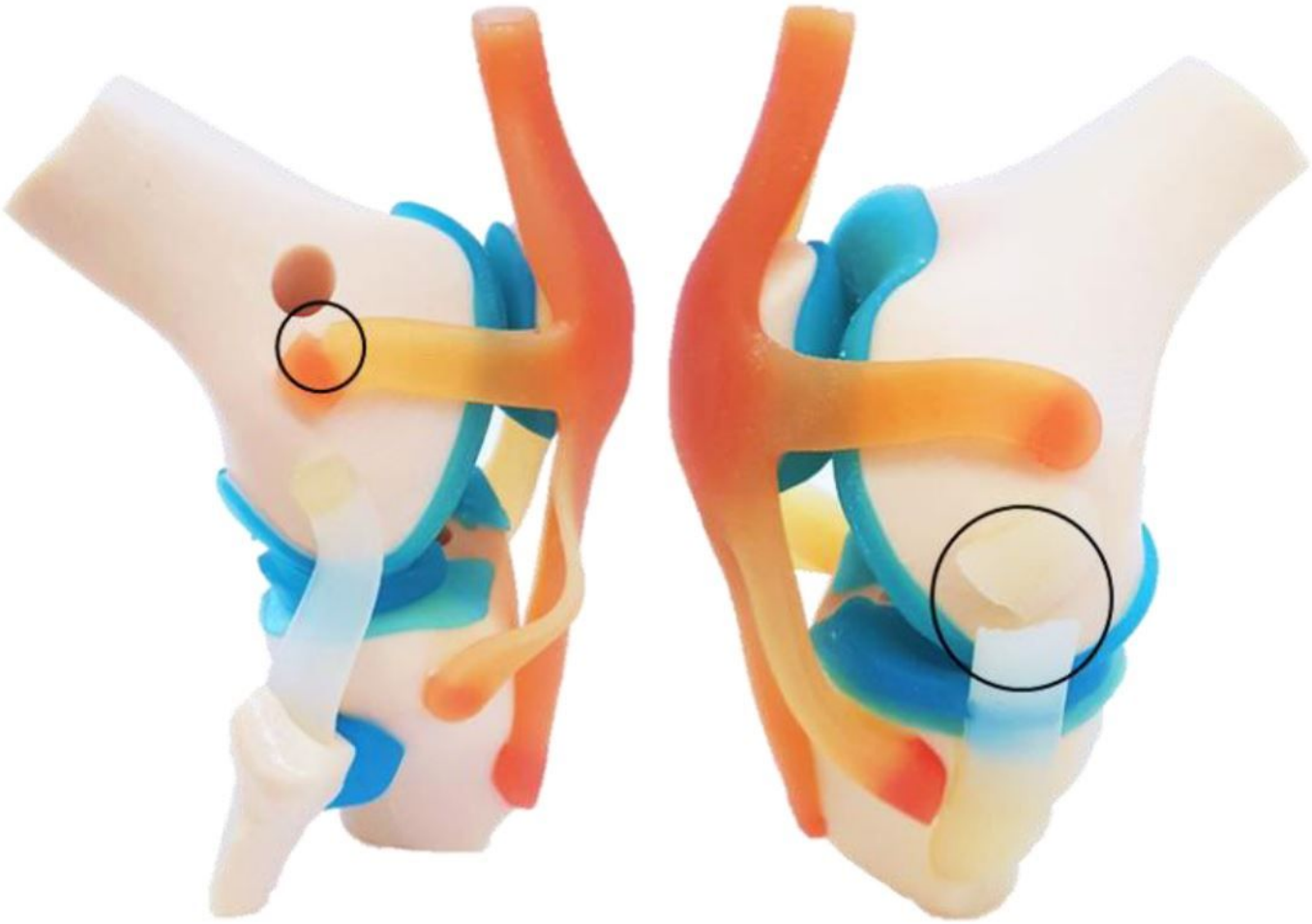

Figure 8

Printing trial scale 1:2. ACL-R model without collagen fibers matrix structure. Knee Joint lateral views in flexion with BPTB graft replacing ACL, rupture of the LPL, and MCL

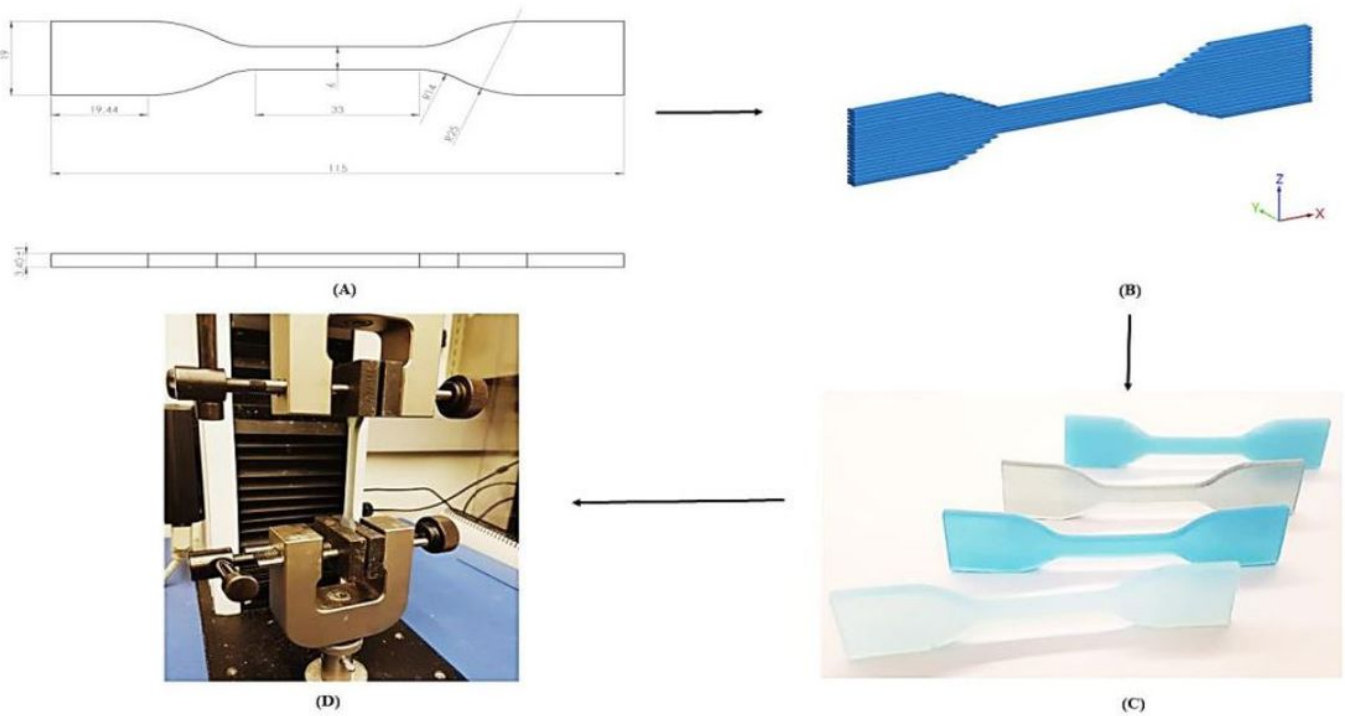

Figure 9

Flowchart application standard D412-C. (A) Dimensions bone specimen (mm), (B) Render bone specimen in SolidWorks software, (C) Printed bone samples with different combinations, (D) Bone specimen attached to a materials testing system Instron S3300 uni-axial testing instrument, to apply tensile load.

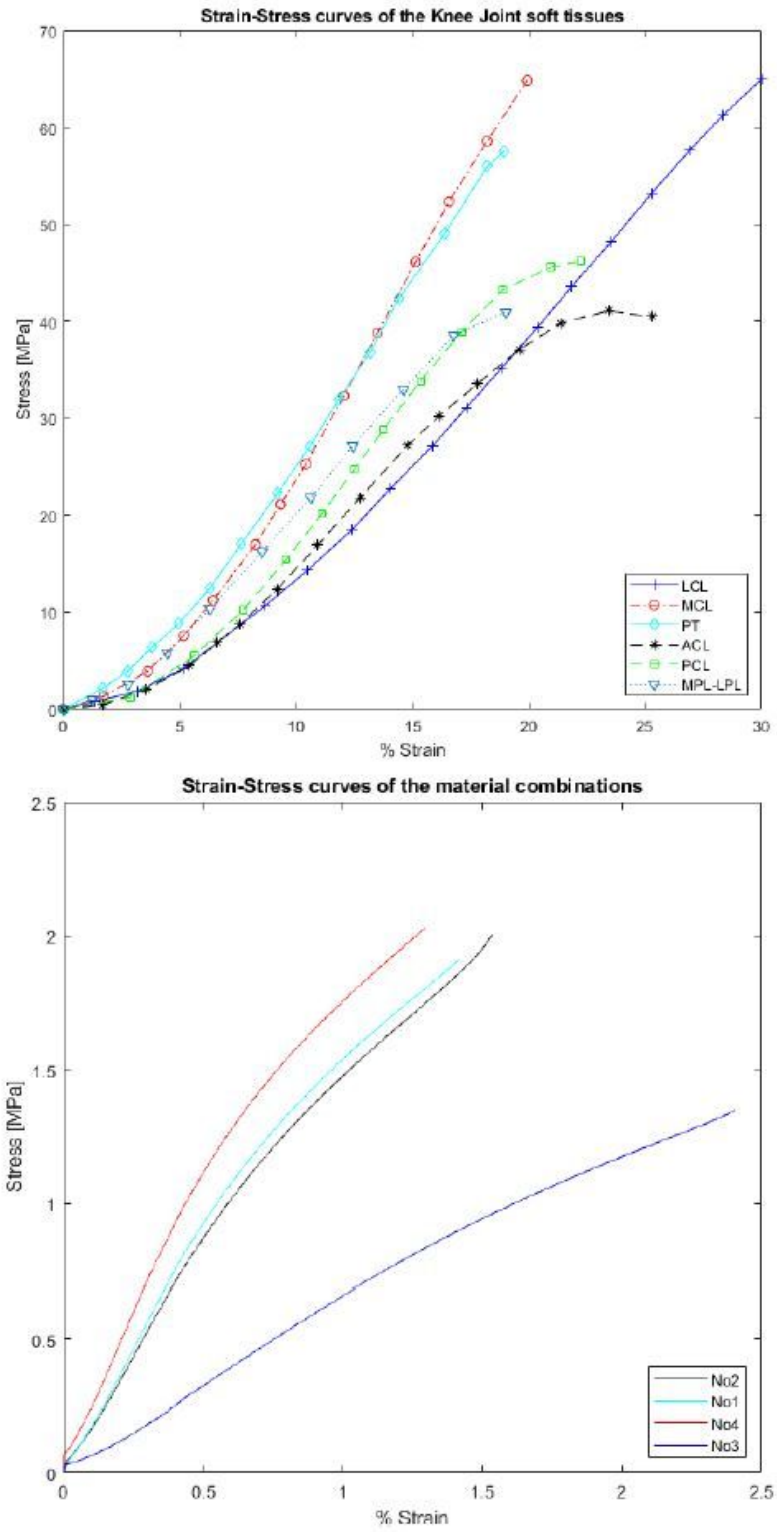

Figure 10

Experimental average Stress-Strain curves of the Knee Joint soft tissues and material combinations.

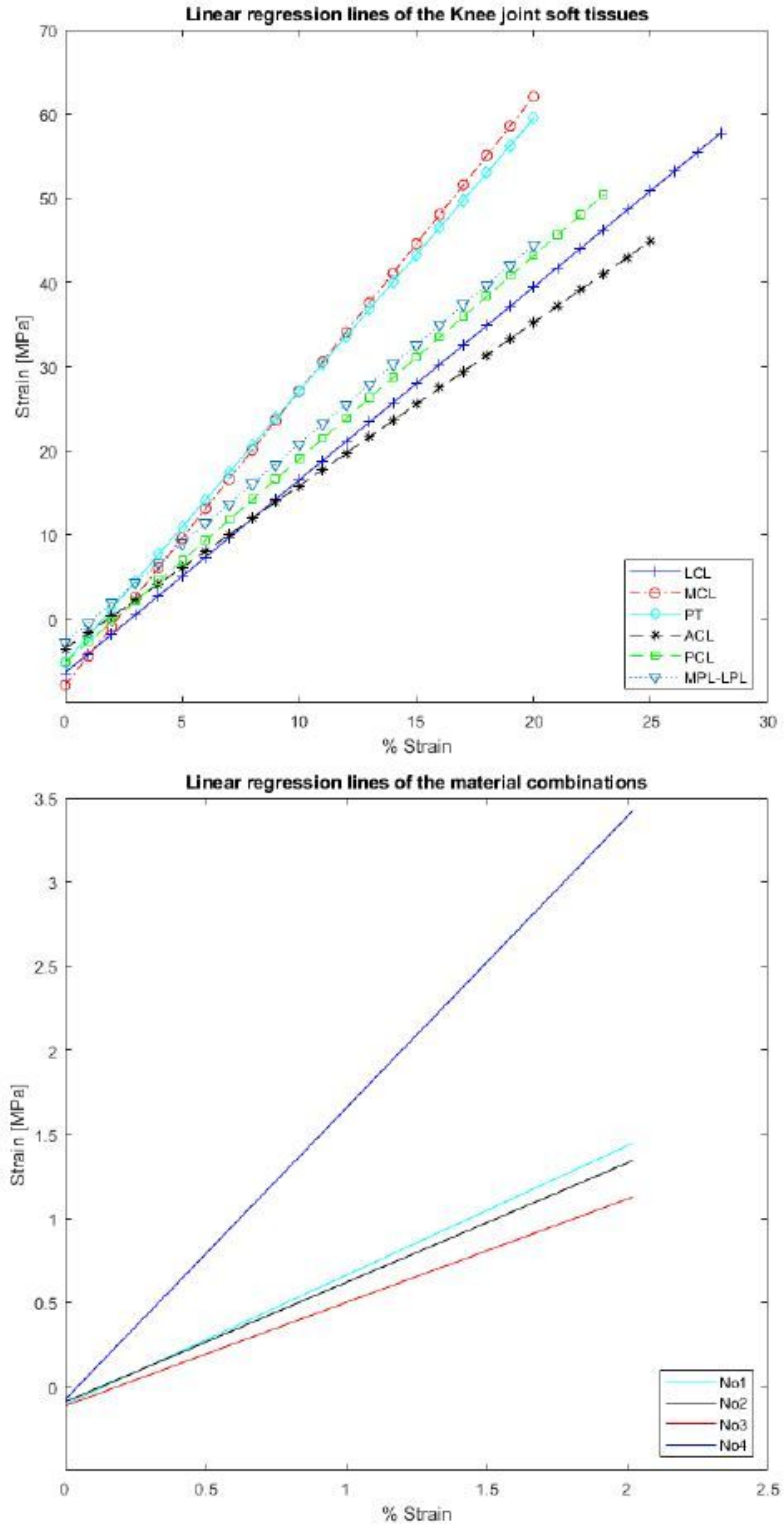

Figure 11

Average linear tendencies for Knee Joint soft tissues and material combinations.

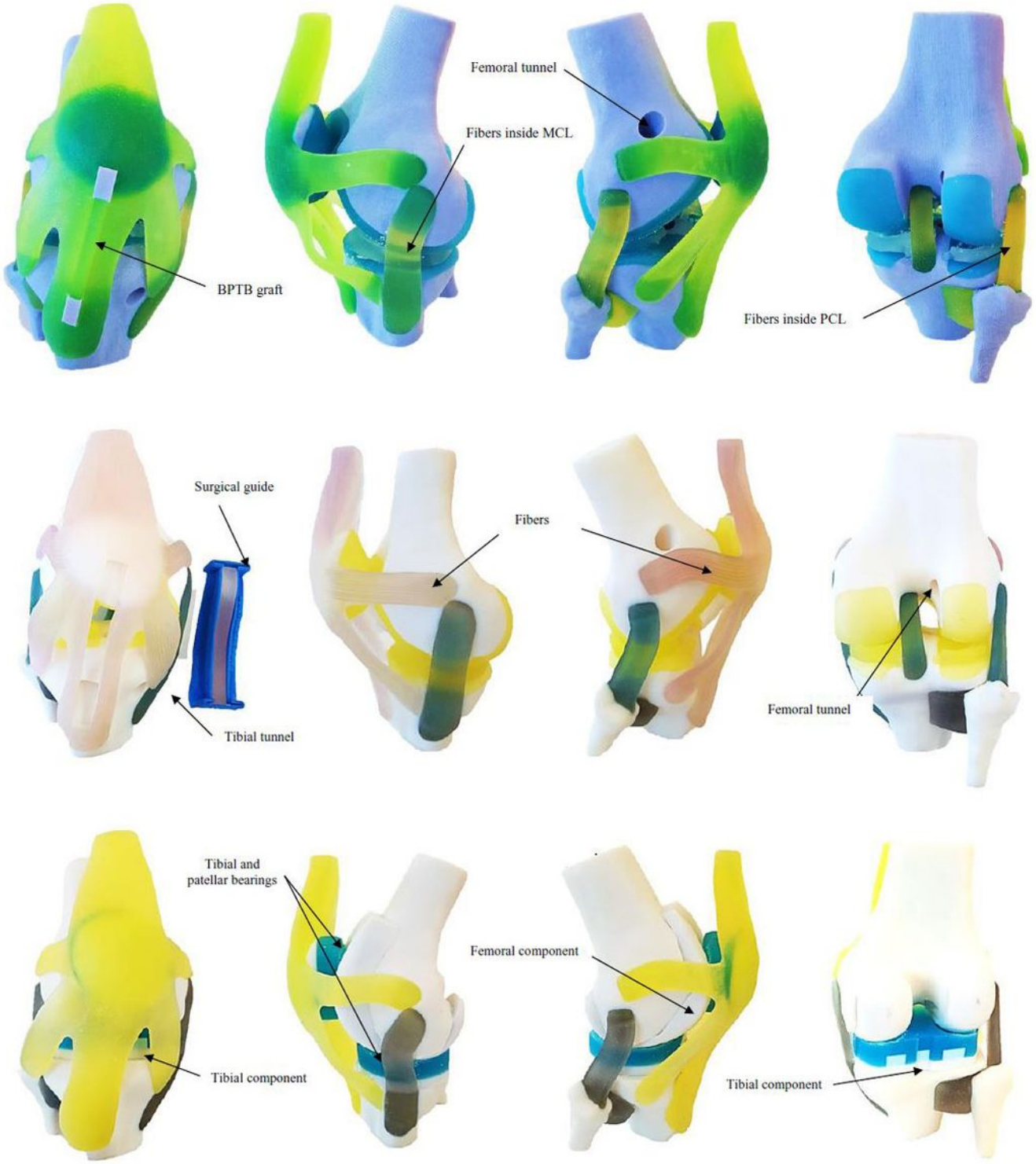

Figure 12

Illustration of Knee Joint PSAMs: (1) Anterior-Lateral- Posterior views of ACL-R (preview study), (2) ACL-R, and (3)TKA models. Final models showed the same details as the 3D computer-generated PSAMs, where the fibers were evident in the grafts and other anatomical structures.

Figure 13

Traditional approach for BPTB autograft harvest using a ruler to measure graft dimension and proposed approach using ACL surgical guide.